이학박사 학위논문

Study of Electron Spin Dynamics of Phosphorus-Doped Silicon

인 도핑된 실리콘에 대한 전자 스핀 동역학 연구

2015 년 7 월

서울대학교 대학원

물리·천문학부

곽 민 찬

Study of Electron Spin Dynamics of Phosphorus-Doped Silicon

인 도핑된 실리콘에 대한 전자 스핀 동역학 연구

지도교수 유 인 석

이 논문을 이학박사 학위논문으로 제출함
2015 년 4 월

서울대학교 대학원
물리·천문학부
곽 민 찬

곽민찬의 박사 학위논문을 인준함
2015 년 7 월

위 원 장 박 제 근 (인)

부위원장 유 인 석 (인)

위 원 제 원 호 (인)

위 원 정 현 석 (인)

위 원 이 상 갑 (인)

Study of Electron Spin Dynamics of Phosphorus-Doped Silicon

Minchan Gwak

Supervised by

Professor Insuk Yu

A Dissertation in Physics

Submitted to the Faculties of
Seoul National University
in Partial Fulfillment of the Requirements for the
Degree of Doctor of Philosophy

July 2015

Department of Physics and Astronomy
The Graduate College of Natural Sciences
Seoul National University

Abstract

Quantum information stored in a quantum bit (qubit), basic element of quantum computation, is fragile to interaction with environments, and disappears with time. To overcome this, quantum error correction technique has been studied and it is known that, if a given requirement is satisfied, it is possible to perform fault-tolerant quantum computation. The requirement is that the number of physical qubits should be able to increase arbitrarily and the error probability per each gate operation should be smaller than a certain level (10^{-4}~10^{-6}). Kane's silicon-based quantum computer, suggested to satisfy the severe requirement of quantum error correction, has attracted particular attention as a promising candidate for practical quantum computer. Regarding this, relatively short coherence time of electron spins in silicon, compared to that of ^{31}P nuclear spins, is a key factor for reliable quantum computation. Previous researches focused on decreasing density of impurities (donor and ^{29}Si) in silicon to increase coherence time of electron spins. However, considering that the speed of two-qubit operation is proportional to exchange constant (J) between electron spins, research for a sample with high donor density is necessary.

In this study, electron spin resonance experiments were performed for

dielectric Si:P with the donor density of $6.52 \times 10^{16}\ /cc$ and 1.1×10^{17} to investigate electron spin dynamics in silicon. Based on the measured relaxation times for electron spins, their relevant mechanisms were elucidated. Furthermore, it was verified if electron spin coherence can be preserved long enough, to satisfy the requirement for fault-tolerant quantum computation, by dynamical decoupling technique. To obtain information for dynamics of single electron spin from measurements on bulk sample, the effect of field inhomogeneity due to ^{29}Si nuclei in silicon was dealt with by spin echo technique, which utilizes refocusing (π) pulse.

For the given experimental condition, the dominant mechanisms for decoherence of electron spins are estimated to be instantaneous diffusion and (^{29}Si) nuclear-induced spectral diffusion. The measured time constants for each mechanism are $0.9\,ms$ (T_{ID}) and $0.26\,ms$ (T_{SD}), respectively. Instantaneous diffusion arises when dipolar-coupled electron spins are simultaneously flipped by an applied microwave pulse. The theoretical formula for T_{ID} agrees with previous experimental results obtained for low donor densities, but shows large discrepancy with our result ($T_{ID,theory} \sim 0.02\,ms$). This can be explained qualitatively by the fact that as donor density increases, the number of exchange-coupled spin pairs, which have exchange constant (J) larger than hyperfine interaction (A) between ^{31}P

and electron, also increases. Meanwhile, spectral diffusion arises when local magnetic field at a resonant spin fluctuates due to lattice-related flips of nearby spins or dipolar flip-flops of nearby spins. By comparing our results of T_{SD} with previous results, it is shown that inhomogeneous field due to the presence of ^{29}Si nuclei suppresses electron-induced spectral diffusion so that (^{29}Si) nuclear-induced spectral diffusion becomes dominant.

In our results of dynamical decoupling experiment to suppress spectral diffusion, the theoretically driven optimal DD sequence (UDD) outperforms the conventional equidistant sequence (PDD) especially at short times, often called high-fidelity regime. This regime is important in quantum error correction and thus these results show that dynamical decoupling can take an important role in quantum computation. From the measured echo decay using UDD with four refocusing pulses, the time taken for error probability to be 10^{-6} is estimated to be about 0.13 ms and this value is comparable to the limit of gate operation time due to the limit of current pulse generation technology.

Keywords : phosphorus-doped silicon, electron spin resonance, spin relaxation, spin echo, decoherence, dynamical decoupling

Student number : 2009-20392

Contents

List of Figures

Chapter 1

Introduction

The element silicon is like 'the giving tree' for human beings. In the form of silicate minerals, composing over 90% of the Earth's crust, silicon is used in almost everything around us, from buildings to glasses, ceramics – the list goes on and on. Highly purified silicon, which can be extracted from sand, also has been very influential on modern technology. It is widely used in integrated circuits, the basis of most electronic devices including cell phones, televisions and computers. In science research field, silicon has provided a number of research topics. Especially when doped with impurities such as phosphorus or arsenic, silicon shows a variety of physical properties depending on impurity density and temperature, which have attracted many researchers over decades. At room temperatures, the donors, group V element dopants, are ionized by thermal energy and thus the unpaired electron moves freely within the silicon lattice, which makes the

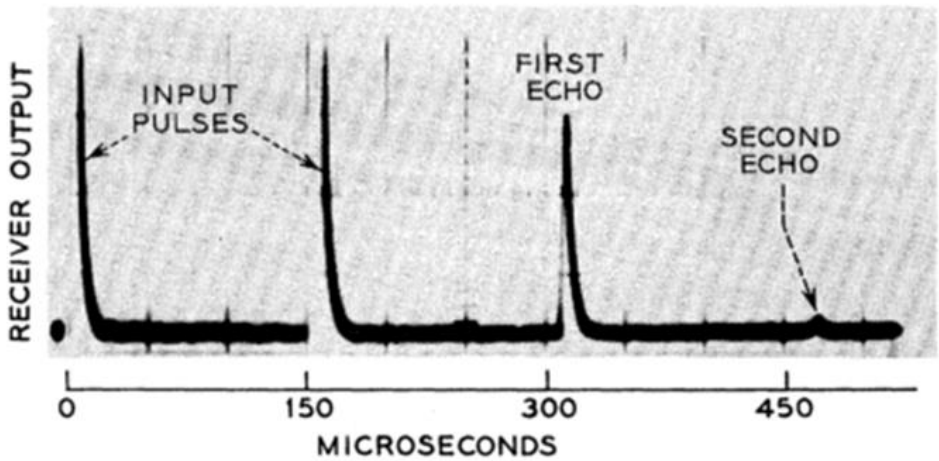

Figure 1.1: The first observed spin-echo signals from phosphorus-doped silicon by pulsed-ESR technique [5].

silicon electrically conductive. On the other hand, at low temperatures and when the donor density is sufficiently low, the unpaired electron is bound to the donor nucleus and the silicon becomes an electrical insulator, that is to say a dielectric. The dielectric silicon has a rich stock of physical information about the interactions between the donor electron and local spins.

One of the successful tools to investigate the physics of bound donor electrons in silicon is electron spin resonance (ESR) spectroscopy which directly measures the energy difference between spin states of unpaired electron in a magnetic field. Fletcher et al. [1] first observed the spin

resonance from bound donor electrons and afterward, Feher and his colleagues accomplished a monumental work on the electronic structure of donors and the electron spin relaxation [2]–[4]. The relaxation of donor electron spins is directly connected to their dynamics under the influence of thermal lattice vibrations (phonons) and other spins. Especially at liquid helium temperatures, the relaxation due to spin–spin interactions, the so-called transverse relaxation, becomes dominant. However the transverse relaxation, which is energy-conserving process by definition, cannot be observed by the conventional continuous wave ESR (CW-ESR) technique measuring the absorbed microwave energy by a sample. With the development of microwave pulse technique, the pulsed-ESR technique enabled researchers to directly investigate the transverse relaxation of donor electron spins. At 1958, Gordon and Bowers first demonstrated the microwave spin echoes from donor electrons in silicon (Fig. 1.1) to measure the transverse relaxation time, for different donor densities and silicon isotope compositions [5]. Afterwards, many researchers have contributed to elucidate the mechanisms responsible for the echo decay behaviors of doped silicon. Among them, Klauder and Anderson laid a foundation of a theoretical description based on a stochastic model [6], and Chiba and Hirai successfully explained the measured echo decay data for different donor

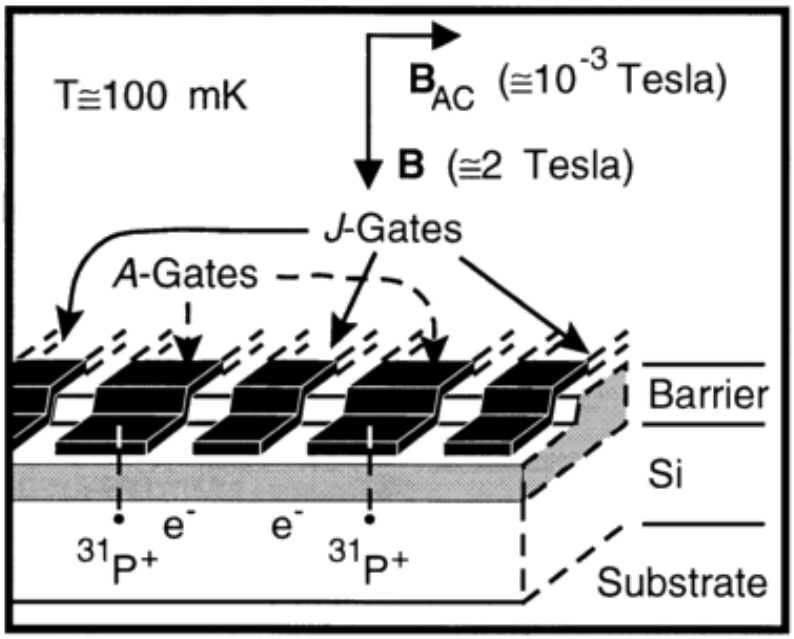

Figure 1.2: The schematic diagram of the Kane quantum computer [8].

densities by using the stochastic model [7]. As a result, at that time of the early 70s, the electron spin echo decay behaviors of doped silicon was considered to be fully understood.

After almost three decades, the transverse relaxation of donor electron spins in silicon begun to attract attention from researchers again. This was sparked by the Kane's proposal [8] (Fig. 1.2) for a Si:P quantum computer to satisfy the severe requirements of quantum error-correction technique which enables reliable quantum computation against inevitable errors. Specific Si-based quantum computer architectures utilize donor nuclear

spins or donor-bound electron spins or both as quantum bits (qubits). Because the transverse relaxation, that is decoherence, of spin qubits implies that the stored quantum information gets lost, relatively short coherence time of electron spins has become one of the main hurdles towards an implementation of Si-based quantum computer. To overcome this, researchers have focused on reducing the density of impurities to increase the coherence time of electron spins [9]-[13]. However, for the elementary two-qubit operation [14]-[16], electron spin qubits should be close enough to each other and thus reducing the donor density cannot be the final solution. This has necessitated a different approach to deal with donor-induced decoherence.

The present thesis is to investigate dielectric Si:P with the donor density, high enough for the exchange coupling between donor electrons to be important, at liquid helium temperatures by ESR technique, elucidate the mechanisms responsible for the decoherence of donor electrons, and report the utility of dynamical decoupling technique which suppresses the spectral diffusion, one of the dominant decoherence mechanisms, to satisfy the error threshold for the fault-tolerant quantum computation.

The thesis continues, in Chapter 2, with detailed descriptions of the background and theory. The topics introduced are: the physical properties

of phosphorus-doped silicon, the basics of ESR and spin relaxations, and silicon-based quantum computer. In subsequent three chapters, experimental results from electron spin resonance experiments of phosphorus-doped silicon will be given. The first of them, Chapter 3, considers the measurement of electronic energy spectrum by electron spin resonance technique. Preliminary results from spectral hole-burning measurements to study the spin dynamics during dynamical nuclear polarization will also be presented. The second, Chapter 4, is on the measurement of electron spin decoherence and the relevant mechanisms. The third, Chapter 5, is about the measurement of prolonged spin coherence by dynamical decoupling (DD). Also are included a novel feature in echo decay regarding instrumental field (or frequency) noise and the evaluation of the performance of DD in the perspective of fault-tolerant quantum computation. The thesis finishes in Chapter 6 with conclusions.

Chapter 2

Background and Theory

Phosphorus-doped silicon, Si:P, has been one of the most extensively studied solid-state system because it shows a variety of physical properties depending on donor density, silicon isotope abundance and temperature. Among many research subjects for Si:P, decoherence of donor electron spins has come into the spotlight since the late 20th century because it plays a significant role in the implementation of silicon-based quantum computers. With no doubt, electron spin resonance (ESR) technique is the most effective tool for investigating decoherence of donor electrons. In this chapter, the physical properties of phosphorus-doped silicon which is essential for the understanding of this thesis will be discussed. The general description of the basics of ESR and spin relaxation will also be discussed. A brief discussion of the requisites for reliable quantum computation and silicon-based quantum computer architectures will close the chapter.

2.1 Phosphorus-doped Silicon

Silicon (Si) has four valence electrons and, in its solid state, all of them participate in forming covalent bonds with the neighboring Si atoms. When a phosphorus atom, which has five valence electrons, substitutes a Si atom in the lattice, four of the valence electrons of phosphorus are used to form covalent bonds and the fifth valence electron acts as an unpaired electron which is weakly bound to the phosphorus nucleus by the Coulomb attraction at low temperatures. This provides a hydrogenic system of a single electron bound to an ionic nucleus in the host material, silicon, as a dielectric medium. The electron wave function and corresponding energy levels of phosphorus in silicon can be considered to be hydrogen-like, but due to the presence of the host material, silicon, consideration of the physical properties of silicon is necessary for a deep understanding of the behavior of the donor electron. This section involves the characteristic of phosphorus-doped silicon especially in the prospect of using it as a host material for quantum computing [17], [18].

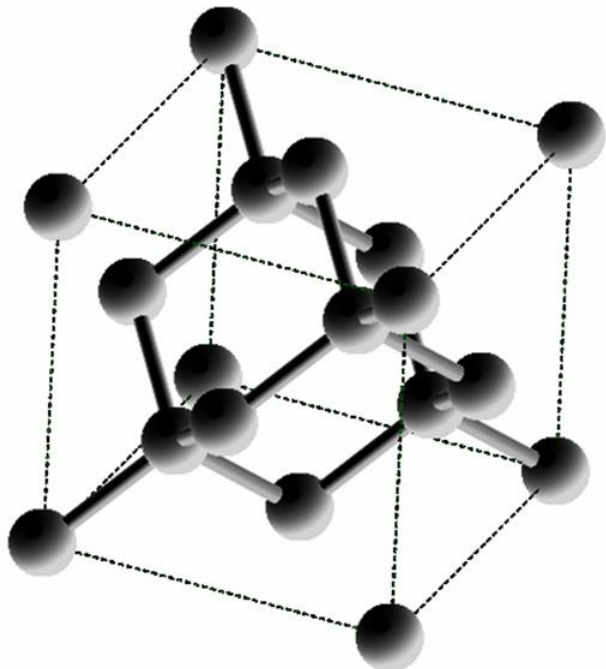

Figure 2.1: The diamond cubic crystal structure of crystalline silicon. Dotted lines represent the unit cell.

2.1.1 Crystalline silicon

In solid state, four valence electrons of silicon contribute to form tetrahedral bonds with its nearest neighbors, which results in a diamond cubic crystal structure (Fig. 2.1). Dotted lines in the figure represent the unit cell with a lattice spacing of 0.543 nm [19].

Silicon has three stable isotopes ^{28}Si, ^{29}Si and ^{30}Si. Their natural abundance and spin quantum number are presented in Table 2.1. Among them, only

^{29}Si has non-zero spin, and thus the isotopic composition of crystalline silicon highly affects the degree of interaction between donor electron and its environment. For instance, decoherence of donor electron spins in phosphorus-doped silicon can be suppressed by eliminating ^{29}Si impurities with the aid of isotopic purification technique [20]. In a commercial silicon wafer with randomly doped phosphorus atoms, each donor electron has its own configuration of nearby ^{29}Si nuclei. Because the ^{29}Si nuclei interact with the donor electron by hyperfine interaction which depends on the relative position of ^{29}Si to the donor, inhomogeneity on electron spin energy levels arises in such sample, which makes it hard to know the Larmor frequency of a specific electron precisely. This leads to severe tuning constraints on one-qubit gate operation in silicon-based quantum computation. Thus in most of silicon-based quantum computer architectures, isotopic enrichment of silicon to extremely reduce the density of ^{29}Si is necessary for almost nuclear spin free environment [21]. Fortunately, it is still possible to build an universal quantum computer only with two-qubit gate operations [15].

Isotope	Nuclear Spin	Natural Abundance
^{28}Si	0	92.23%
^{29}Si	+1/2	4.67%
^{30}Si	0	3.1%

Table 2.1: Stable isotopes in silicon

2.1.2 Donor wave function

Because donor electron resides in the silicon lattice, its wave function is different from that of hydrogen atom. In the effective mass theory which involves electron wave function in a periodic potential, the mass of the electron is considered to be changed from the free electron mass to an effective mass, and the donor electron wave function is expressed by an linear combination of the periodic Bloch functions for silicon lattice structure [3], [22], [23]. The ground state wave function of the bound donor electron in silicon, often called Kohn–Luttinger wave function, has the form:

$$\psi(\mathbf{r}) = \frac{1}{\sqrt{6}}\sum_{j=1}^{6} F^{(j)}(\mathbf{r})u^{(j)}(\mathbf{r})\exp(i\mathbf{k}_0^j \cdot \mathbf{r}), \qquad (2.1)$$

where $u^{(j)}(\mathbf{r})\exp(i\mathbf{k}_0^j \cdot \mathbf{r})$ is the Bloch function at the jth conduction band minimum and $F^{(j)}(\mathbf{r})$ is a hydrogenic envelope function obtained by solving

an Schrödinger equation with the effective mass. The Bohr radius of the envelope function is estimated to be about 25 nm [23], [24]. The calculated wave function is shown in Fig. 2.2. The wave function oscillates in intensity with distance from the core because of inter-valley interference between six degenerate conduction band minima [25]. Also the shape of this interference is different along different directions in the crystal. This leads to oscillations in the exchange interaction between neighboring donor electrons in silicon with the distance and the relative orientation between them, which plays a crucial role in the construction of silicon-based quantum computer [25], [26].

2.1.3 Hyperfine interaction

In phosphorus-doped silicon, bound donor electron interacts with its own donor nucleus, ^{31}P, by contact-type hyperfine interaction, or Fermi contact interaction. This is because the ground state wave function is s-like which renders a non-zero probability density at the center, the position of ^{31}P (see Fig. 2.2). Here the strength of the interaction between them can be described by the following equation:

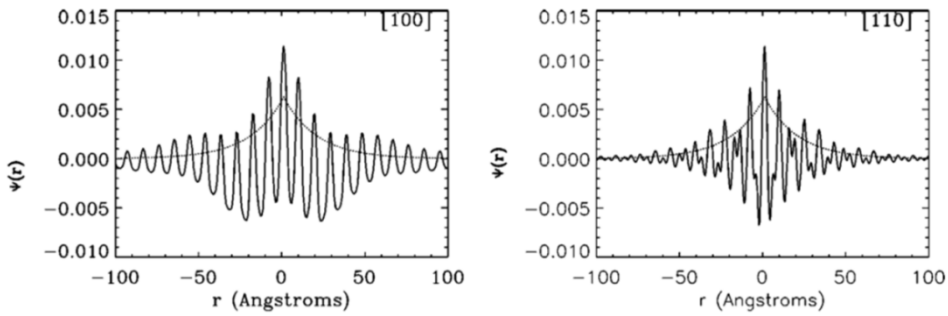

Figure 2.2: Effective-mass wave function of phosphorus donor electron along the (100) and (110) direction of the silicon lattice. The exponential decay line shows an isotropic 1s hydrogenic wave function with a Bohr radius of 20.13 Å [25].

$$\mathrm{H_{FC}} = \frac{8\pi}{3}\gamma_n\gamma_e\hbar^2|\psi(0)|^2\boldsymbol{I}\cdot\boldsymbol{S}, \tag{2.2}$$

where $\boldsymbol{I}$ and $\boldsymbol{S}$ are the nuclear and electron spin operators respectively, γ_n and γ_e the gyromagnetic ratios of nuclear and electron spin respectively and $|\psi(0)|^2$ the probability density of the electron at the ^{31}P nucleus. The magnitude of the interaction can be measured with electron spin resonance technique and is about 42 G [7].

The donor electron also interacts with nearby ^{29}Si nuclei by hyperfine interaction. For ^{29}Si nuclei inside the electron wave function, the interaction is contact type and can be expressed by Eq. (2.2) where $|\psi(0)|^2$ is replaced by $|\psi(\mathbf{r}_i)|^2$. Here $\mathbf{r}_i$ represents the relative position of the ith ^{29}Si nucleus to the donor. On the other hand, for ^{29}Si nuclei outside the electron wave

function, the interaction is given by the dipolar interaction at finite distance:

$$H_D = \frac{\mu_0 \gamma_n \gamma_e \hbar^2}{4\pi} \sum_i \frac{1}{|\mathbf{r}_i|^3} \{3(\boldsymbol{I} \cdot \hat{\mathbf{r}}_i)(\boldsymbol{S} \cdot \hat{\mathbf{r}}_i) - \boldsymbol{I} \cdot \boldsymbol{S}\}, \quad (2.3)$$

where μ_0 is the magnetic permeability of vacuum. These interactions induce inhomogeneous magnetic fields to donor electrons because ^{29}Si nuclei are randomly distributed in silicon. The inhomogeneity manifests itself as a broadening of resonance lines in electron spin resonance spectrum of Si:P and is experimentally measured to be about 2.5 G [7].

2.1.4 Exchange interaction

The exchange interaction arises from the characteristic of the wave function of two identical particles regarding the exchange operator which exchanges the position of the particles. In other words, the wave function must obey the symmetrization requirement under the exchange operation. Let's consider a two-electron system. Because electron is a fermion, the wave function, representing the electrons at position $\mathbf{r_1}$ and $\mathbf{r_2}$, must be antisymmetric under the exchange operation:

$$\psi(\mathbf{r_1}, \mathbf{r_2}) = -\psi(\mathbf{r_2}, \mathbf{r_1}). \quad (2.3)$$

The electron wave function $\psi(\mathbf{r_1}, \mathbf{r_2})$ consists of both spatial (ψ_r) and spin (χ_s) states. Among them, the spin state can be described by a singlet

state with total spin quantum number $S = 0$ and triplet states with $S = 1$:

$$S = 1 \quad \begin{cases} |\uparrow\uparrow\rangle \\ \frac{1}{\sqrt{2}}(|\uparrow\downarrow\rangle + |\downarrow\uparrow\rangle) \\ |\downarrow\downarrow\rangle \end{cases} \tag{2.4}$$

$$S = 0 \quad \frac{1}{\sqrt{2}}(|\uparrow\downarrow\rangle - |\downarrow\uparrow\rangle). \tag{2.5}$$

The singlet state is antisymmetric under the exchange operation and the triplet states are symmetric. To satisfy the symmetry requirement, Eq. (2.3), one of the spin state and the spatial state must be antisymmetric and the other symmetric. Thus the spin singlet state (antisymmetric) must go with a symmetric spatial state, and the triplet spin state (symmetric) an antisymmetric spatial state.

Comparing with the case that there is no exchange interaction, the electrons sit further apart for antisymmetric spatial states. Otherwise, the electrons sit closer together for symmetric spatial states. This leads to larger overlap of electron wave functions for the singlet spin state than the triplet, and consequently the singlet has lower energy than the triplet. Here the difference in energy is represented by the exchange constant J. As a result, the singlet spin state becomes a ground state with the energy lower than that of the triplet spin states by J [27].

In the presence of an external magnetic field, the degeneracy of the triplet states is lifted by the Zeeman effect as shown in Fig. 2.3. Here the Zeeman

splitting of an electron in a magnetic field B_0 is labelled as ω_S, that is to say $\omega_S = \gamma_e B_0$ where γ_e is the electron gyromagnetic ratio. If the exchange constant J is much larger than ω_S, the singlet state will be still the ground state. This has important implication on ESR measurements for doped silicon with the donor density high enough to contain many exchange-coupled electron pairs. Because the singlet spin state $(S = 0)$ cannot be excited by microwave, and thus is irrelevant to ESR, it is expected that an effective donor density which contributes ESR will be considerably lower than the total donor density in the sample with high donor density. Fig. 2.4 shows the calculated distribution of nearest-neighbor exchange couplings for two values of donor density n_D, $1 \times 10^{17}\ /cc\ (n_D a^2 b = 0.0005)$ and $8 \times 10^{17}\ /cc\ (n_D a^2 b = 0.003)$ where a and b represent the Kohn-Luttinger radii [28]. For instance, considering a conventional W-band ESR in which ω_S is about 100 GHz ($\sim 1.5 \times 10^{-5}$ hartree), about 60 % of donor pairs have the exchange constant J larger than ω_S for the donor density of $1 \times 10^{17}\ /cc$. In Chapter 4, it will be shown that the decrease in an ESR-effective donor density can affect the spin decoherence time of donor electron.

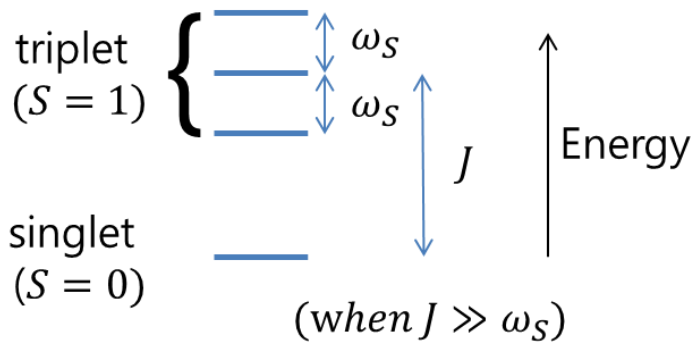

Figure 2.3: Energy diagram for an exchange-coupled electron pair with the exchange energy J much larger than electron Zeeman splitting $\boldsymbol{\omega_S}$ in a magnetic field.

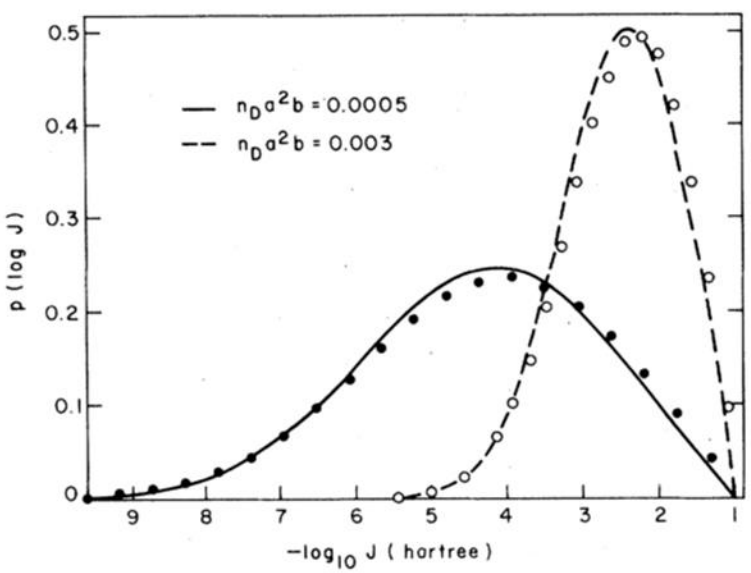

Figure 2.4: Calculated distribution of nearest-neighbor exchange couplings $\boldsymbol{p(\ln J)}$ for isotropic (circles and points) and anisotropic exchange interactions (appropriate for Si:P, dashed and solid lines) for two values of $\mathbf{n_D a^2 b}$, as indicated [44].

2.2 Electron Spin Resonance

Electron spin resonance (ESR) or electron paramagnetic resonance (EPR) is a physical phenomenon in which electron in a magnetic field absorbs and re-emits electromagnetic radiation with a specific resonance frequency. The photonic energy of the resonant radiation corresponds to the Zeeman splitting of the electron spin, which depends on the strength of the magnetic field and the gyromagnetic ratio of the electron (Fig. 2.5). Here the magnetic field consists of an applied external field and an internal field due to nearby spins. Thus ESR can be utilized for spectroscopy, investigating the structure of electronic spin energy levels. ESR spectroscopy has a variety of applications, from studying metal complexes or organic radicals to obtaining information about the interactions between donor electrons and other paramagnetic impurities in semiconductors.

2.2.1 Spin populations

The resonant electromagnetic radiation induces transitions between energy levels in both directions, from lower to higher energy level, and vice versa. Thus if the electron populations of both levels are same in bulk sample, there will be no net change of energy during ESR and consequently no ESR

signal. Fortunately, at finite temperatures, it is not the case. When an electron ensemble in a sample is in thermodynamic equilibrium with its environment acting as a thermal bath, its statistical distribution follows the Maxwell–Boltzmann distribution and the ratio of the populations of the upper and lower energy levels is given by the Boltzmann factor:

$$\frac{n_{upper}}{n_{lower}} = \exp\left(\frac{-E_{upper}-E_{lower}}{kT}\right) = \exp\left(-\frac{\Delta E}{kT}\right) \quad (2.5)$$

where n_{upper} (n_{lower}) is the number of electrons occupying the upper (lower) energy state, k is the Boltzmann constant, and T is the temperature. The temperature dependence of the population ratio between Zeeman energy levels of free electrons at some values of magnetic field is shown in Fig. 2.6. At finite temperatures ($T > 0$), the upper energy level clearly has a smaller population than the lower one, that is to say $\frac{n_{upper}}{n_{lower}} < 1$. Thus, transitions from the lower to the upper level are more probable than the reverse during ESR, which results in the net absorption of energy by a sample. Thus it is possible to measure ESR absorption spectrum by the conventional continuous wave ESR technique. Meanwhile, the difference between populations leads to the non-zero net magnetization vector of the electron spins. The net magnetization can be manipulated by pulsed ESR technique to obtain the information about spin dynamics as discussed in the next section.

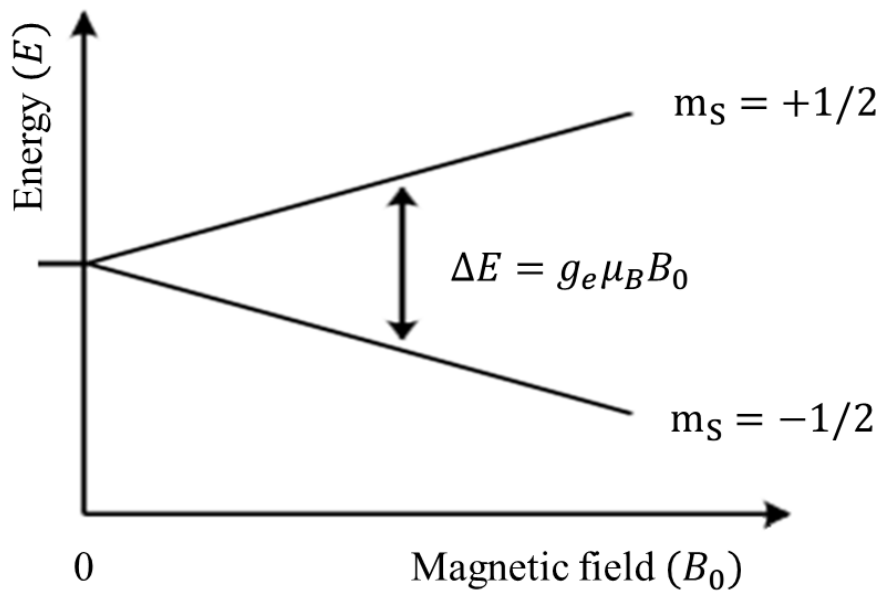

Figure 2.5: The splitting of the electronic energy levels in a magnetic field, where $\mathbf{m_S}$ is the magnetic quantum number, $\boldsymbol{g_e}$ the electron's g−factor and $\boldsymbol{\mu_B}$ the Bohr magneton. The upper line ($\mathbf{m_S = +1/2}$) corresponds to the antiparallel alignment of the electron's magnetic moment to an external magnetic field while the lower line ($\mathbf{m_S = -1/2}$) does to the parallel alignment.

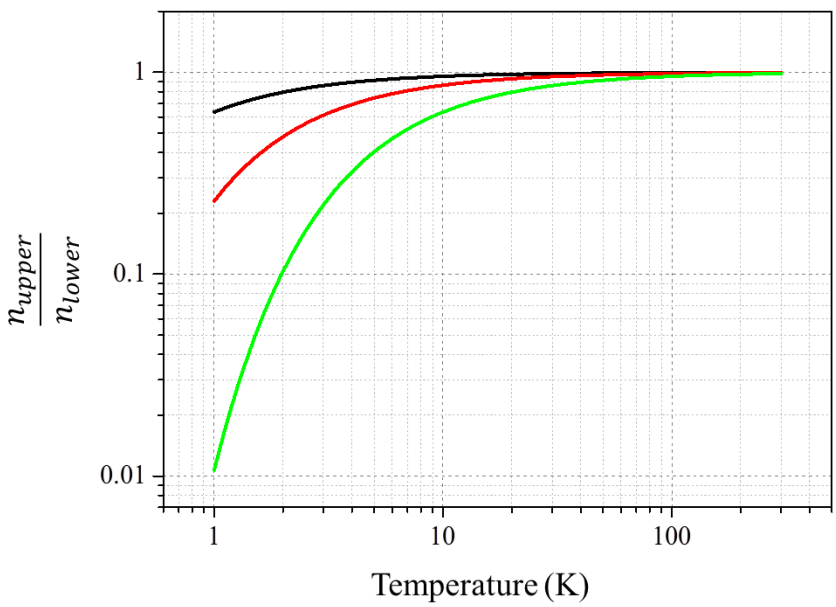

Figure 2.6: The temperature dependence of the population ratio between Zeeman energy levels of free electrons at the magnetic field of 0.34 T (black), 1.1 T (red), and 3.3 T (green).

2.2.2 Pulsed ESR

Pulsed electron spin resonance (ESR) is an electron spin resonance technique that manipulates the net magnetization vector of the electron spins which originally aligned parallel to an external magnetic field. This is performed by applying a resonant electromagnetic radiation, usually with frequencies in microwave regime, to sample for short time. For two level systems like electron in a magnetic field, the transition probability between states induced by a resonant oscillating field is given by the well-known equation for Rabi oscillation [29]:

$$P(t) = \sin^2(\frac{\gamma B_1 t}{2}). \quad (2.6)$$

where γ is the gyromagnetic ratio of particle and B_1 the strength of the oscillating magnetic field. Thus it is possible to control precisely the state of an electron spin as long as γ and B_1 are known. This makes pulsed ESR technique special in quantum computing which necessitates precise control of spin qubits. In usual pulsed ESR measurements, a microwave pulse is applied to an electron ensemble in a bulk sample, and then the microwave signal generated by the transverse component of the magnetization, perpendicular to the external magnetic field, is measured. The signal decays with time because the transverse magnetization becomes smaller due to

various interactions inside the sample. Therefore, measured signals contain structural and dynamical information about the sample. In particular, Fourier transformation of the measured signal in the time domain renders an ESR spectrum in the frequency domain. In the thesis, we use pulsed ESR technique as a main tool for studying dynamics of electron spins in a sample.

Microwave pulses which manipulate the magnetization are often named by their tip angles, and the most commonly employed tip angles are $\pi/2$ (90 degrees) and π (180 degrees). A $\pi/2$ pulse tips the magnetization into the x-y plane, and is also called a saturating pulse because the magnetization along the z axis becomes zero, i.e. the populations of parallel and antiparallel states become equal to each other. On the other hand, a π pulse is called an inversion pulse, because it tips the magnetization 180 degrees, exchanging the populations of the spin states (Fig. 2.7). Right after tipping the magnetization into the x-y plane using a $\pi/2$ pulse, the magnetization is stationary in the frame rotating at the frequency of resonant microwave pulse, that is the Larmor frequency of electrons, and the resonant spins have a coherent phase, that is to say the spins are in a pure state. However, because the electron spins interact with their environments, the transverse magnetization will decay with time and finally the system will establish thermal equilibrium with the environments again.

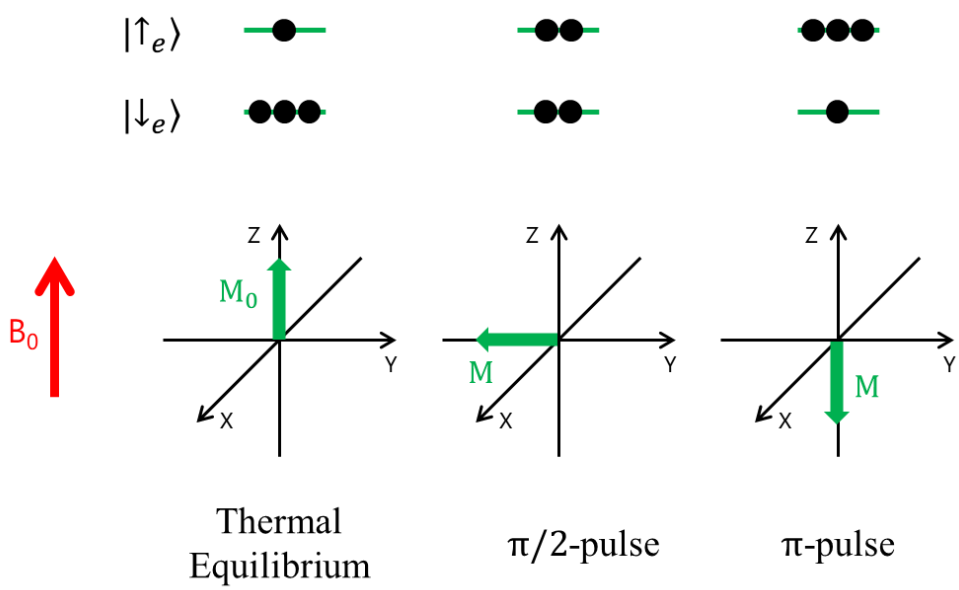

Figure 2.7: Populations of spin states and corresponding magnetizations at thermal equilibrium or right after the application of common pulses.

This process is called relaxation. The decay of the transverse magnetization, which precesses around a static magnetic field at the Larmor frequency in the Lab frame, generates ESR signal. In most cases, the measured signal contains only information about inhomogeneity on the Larmor frequencies of electrons in sample. To obtain the veiled information about spin dynamics, a special pulse technique, often called spin echo, is needed. Before discussing the spin echo in detail, the discussion about the relaxation processes will be given in the following section to start with.

2.3 Spin Relaxations

After a resonant microwave pulse perturbs a system of electron ensemble, the system will interact with its environments and finally return to thermal equilibrium. This process, relaxation, is classified by two different mechanisms, the longitudinal relaxation and the transverse relaxation, which concern the behavior of the longitudinal and transverse components of the net magnetization, respectively.

2.3.1 Longitudinal relaxation

Longitudinal relaxation, or spin–lattice relaxation, is the mechanism by which the longitudinal component of the magnetization along the direction of the external magnetic field is recovered to that of thermal equilibrium with the lattice. This mechanism characterized by the longitudinal relaxation time T_1 which represents how fast the magnetization recovers its longitudinal component. In other words, T_1 is the time in which the energy absorbed from the resonant microwave is dissipated to the lattice as the system returns to thermal equilibrium. The time dependence of the longitudinal magnetization $\mathbf{M_z}$ by longitudinal relaxation is represented by the equation:

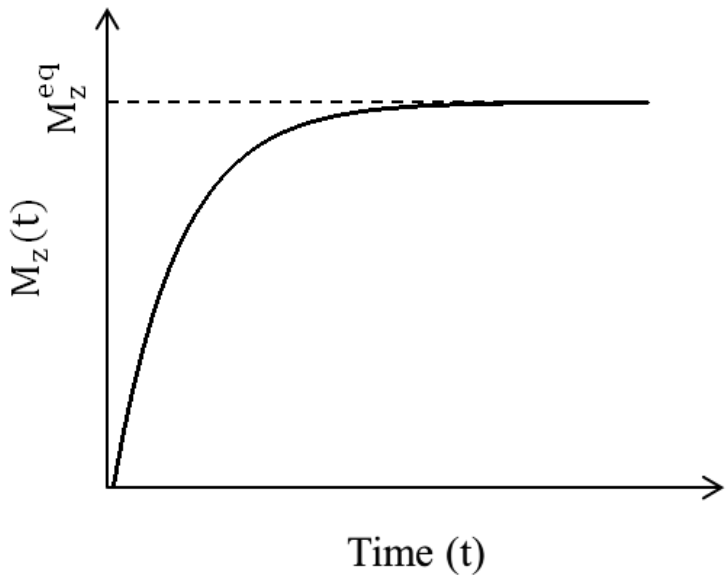

Figure 2.8: Recovery of the longitudinal magnetization with time by longitudinal relaxation.

$$M_z(t) = M_z^{eq} - \{M_z^{eq} - M_z(0)\}e^{-t/T_1}, \quad (2.7)$$

where M_z^{eq} is the longitudinal magnetization at equilibrium. For instance, in the specific case of applying a $\pi/2$ pulse at $t = 0$, $M_z(0) = 0$, and thus

$$M_z(t) = M_z^{eq}(1 - e^{-t/T_1}). \quad (2.8)$$

Fig. 2.8 shows schematically the behavior of the longitudinal magnetization by longitudinal relaxation.

For phosphorus-doped silicon, the mechanisms relevant to longitudinal relaxation of donor electron are well established. Since the first measurement

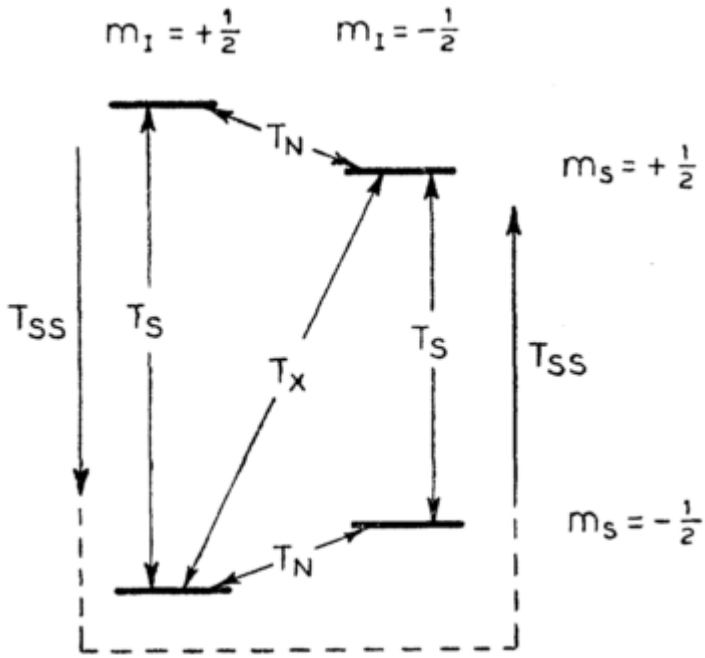

Figure 2.9: Various relaxation mechanisms in a system with $\mathbf{I} = \frac{1}{2}, \boldsymbol{S} = \frac{1}{2}$ which corresponds to phosphorus doped silicon [2].

of relaxation time on donors in silicon by Honig [30], many researchers had contributed to the understanding of electron spin relaxation processes. After the theoretical work of Pines, Bardeen, and Slichter [31], and Abrahams [32], relaxation mechanisms that connect the energy levels in phosphorus doped silicon were elucidated on the basis of the measured relaxation times in the monumental work of Feher and Gere [2] (see Fig. 2.9). They utilized a continuous wave ESR technique, often called an adiabatic fast passage [33], to perturb the spin system. Afterwards, the development of pulsed ESR

technique enabled thorough study of longitudinal relaxation mechanisms. Detailed discussion for the mechanisms at high magnetic field will be given with the measured T_1 data in chapter 4.

2.3.2 Transverse relaxation

Transverse relaxation, or spin–spin relaxation, is the mechanism by which the transverse component of the magnetization perpendicular to the external magnetic field dissipates. This mechanism characterized by the transverse relaxation time T_2 which represents how fast the transverse magnetization decays. Fundamentally, transverse relaxation is due to random fluctuations of the local magnetic field at resonant spins, which leads to fluctuations of instantaneous Larmor precession frequency. This results in the loss of the initial phase coherence among resonant spins and consequently the decay of transverse magnetization. This process is irreversible, that is we cannot recover the lost coherence.

In quantum computing, (quantum) information is stored in the phase of a superstition state of qubit. Transverse relaxation thus limits lifetimes of quantum information in quantum computing which utilizes spins as qubits. This aroused researcher's interest in the transverse relaxation time, or

coherence time, of donor electrons in phosphorus-doped silicon which was suggested by Kane as promising material for a scalable solid-state quantum computer [8]. Due to a sensitivity limitation of ESR technique, measurements of relaxation times, in most cases, are done on a bulk sample which contains an ensemble of electrons. In this case, it is important to check that results of measurements on a bulk sample represent the characteristic of single electron spin properly. This is related to homogeneity of donor's environment inside sample.

In an ideal case of perfect homogeneity in local magnetic fields at resonant spins, that is all resonant spins have the same Larmor frequency, the time dependence of the transverse magnetization M_{xy} by transverse relaxation follows single exponential decay:

$$M_{xy}(t) = M_{xy}(0)e^{-t/T_2}. \quad (2.9)$$

And the measured T_2 on a bulk sample represents the coherence time of single electron spin. However, in most cases, resonant spins in a sample are actually subjected to different chemical or structural environments and thus experience different local magnetic fields. In this case, the inhomogeneity of local magnetic field leads to additional decay of the transverse magnetization. Thus to remove the effect of the inhomogeneity and consequently measure the coherence time of single electron spin from a bulk sample, a special

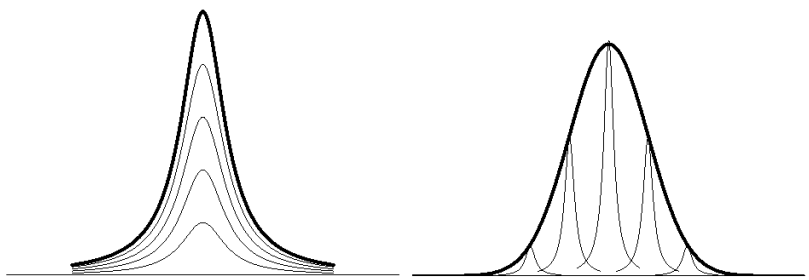

Figure 2.10: Homogeneous broadening (left), and inhomogeneous broaden (right). The inhomogeneously broadened line consists of homogeneously broadened lines.

technique of pulsed ESR, called spin echo, is needed. A detailed discussion on spin echo will be given at section 2.3.4. Before moving on to discuss about spin echo, we will present how homogeneity of donor's environment in a bulk sample affects the shape of ESR lines in the next section. This can help understanding spin echo technique.

2.3.3 Line broadening

ESR lines are broadened by two different mechanisms: homogeneous and inhomogeneous broadening. In a case of homogeneous broadening, a line in ESR spectrum consists of many component lines which are identical to

each other, that is to say all component lines have the same Larmor frequency and linewidth (Fig. 2.10). This implies that all electrons in a sample experience the same magnetic field. Here the linewidth is determined by the uncertainty principle on the limited lifetime of spin states. As shown in previous sections, the lifetime of spin states is limited because the spins interact with each other and their environments, resulting in mutual spin flip-flops and random spin flips, respectively. Thus T_1 and T_2 relaxations both contribute homogenous broadening. This also is related to an exponential decay of the transverse magnetization (Eq. 2.9).

On the other hand, in a case of an inhomogeneous broadening, the spins in a bulk sample experience different local magnetic fields. This occurs, for example, due to inhomogeneity in the external magnetic field and unresolved hyperfine structure. As shown in Fig. 2.10, an inhomogeneously broadened line consists of unresolved spin packets that are themselves homogeneously broadened and have slightly different Larmor frequencies with respect to each other. When the spins are excited by a microwave pulse, the difference in Larmor frequencies leads to a destructive interference of component magnetizations and consequent decrease in the net transverse magnetization. When this happens, the transverse relaxation in a bulk sample is described by the effective transverse relaxation time T_2^*:

$$(T_2^*)^{-1} = (T_2)^{-1} + (T_{inhom})^{-1} = (T_2)^{-1} + \gamma \Delta B_0 \quad (2.10)$$

where γ is gyromagnetic ratio and ΔB_0 the standard deviation of local magnetic field distribution. Also the time dependence of the net magnetization is not an exponential decay, unlike the case of homogeneous broadening, but rather reflects the shape of the EPR spectrum. In phosphorus-doped silicon, ^{29}Si nuclei are randomly distributed, and thus lead to inhomogeneous broadening of ESR lines by hyperfine coupling to donor electrons.

2.3.4 Spin echo

While homogeneous broadening is related to random and irreversible loss of spin states, the decay of the net magnetization due to inhomogeneous broadening is reversible, that is to say it is possible to recover the net magnetization. In a case of inhomogeneous broadening, the disappeared net magnetization can be brought back by an additional pulse, often called refocusing pulse. If the refocusing pulse is applied at a time τ after the first pulse which excited the spins, then the recovered magnetization will be maximized at time τ after the refocusing pulse. This manifests itself as an echo signal (Fig. 2.11). Thus the amplitude of echo signal represents the

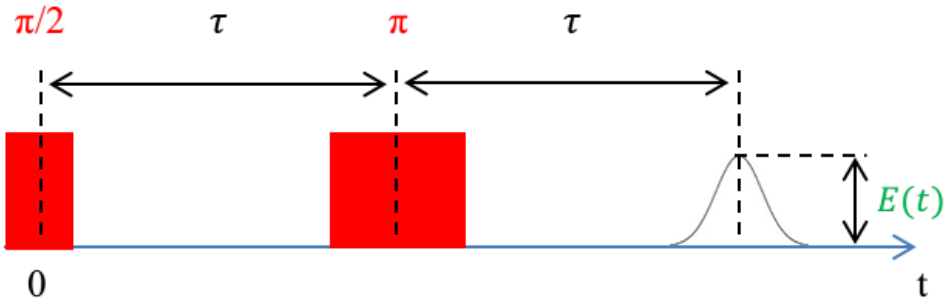

Figure 2.11: Formation of spin echo by a refocusing pulse (π). The echo amplitude $\boldsymbol{E(t)}$ represents the remaining transverse magnetization free from the effect of inhomogeneous broadening.

transverse magnetization of single spin packet remaining at that time, free from the effect of inhomogeneous broadening.

However, the decay of echo amplitude is usually related to not only the transverse relaxation time T_2, but also more contributions such as spin diffusion, spectral diffusion and instantaneous diffusion. Therefore the time constant for echo decay is often called the phase memory time, or T_M, differentiated from T_2. In particular, for phosphorus-dope silicon, spectral diffusion and instantaneous diffusion can dominate the echo decay. These mechanisms induce time-dependent fluctuation of local magnetic fields and thus prevent the perfect refocusing of the net magnetization by π-pulse. This results in additional decay factor in the echo decay curve. More detailed discussion on these mechanisms will be given in chapter 4.

Chapter 3

Electron Spin Resonance in Si:P

3.1 Overview

In this chapter, a preliminary result on dynamic nuclear polarization (DNP) of Si:P will be presented. A CW-ESR experiment was carried at the Turku Atomic Hydrogen Group which is a part of the Wihuri Physical Laboratory of the Department of Physics and Astronomy, University of Turku, Finland. The main type of the experiment was burning the holes in the inhomogeneously broadened ESR lines of Si:P and measuring the hole relaxation. It was found that burning the hole can be easily done even with very small excitation powers (estimated to be hundreds of nW) during several tens of seconds, and with high power during very short times of the order of few seconds. From the change of the ESR spectrum after burning the hole, DNP of ^{31}P and ^{29}Si was identified. A possible explanation for the dependence of the measured DNP build-up times on the excitation (pumping) power will be given. This involves mechanisms of spin diffusion

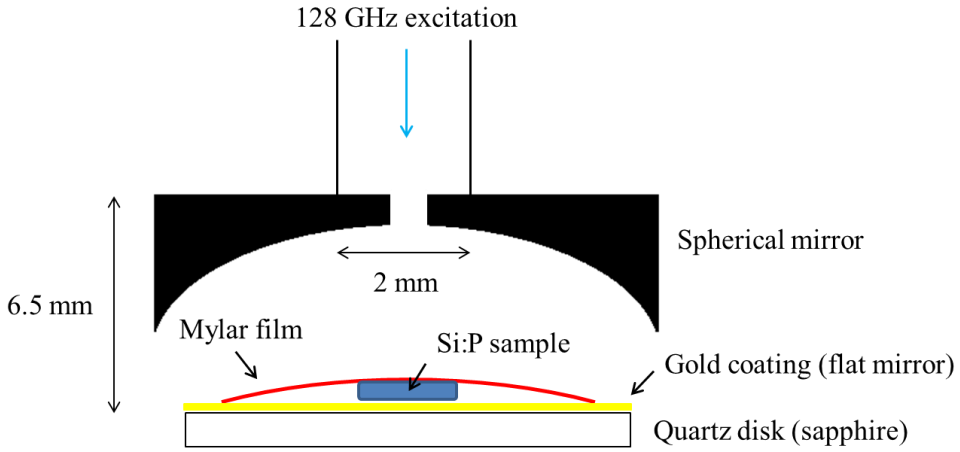

Figure 3.1: Schematic diagram for the experimental setup. The sample was pressed by the Mylar film onto the flat mirror. The cavity was tuned to operate at TEM_{006} mode and frequency of 129.1 GHz.

inside the silicon which propagate enhanced nuclear polarization to the bulk of the sample. Expetimental findings on the relaxation of DNP will be also given.

3.2 Experimental details

We performed CW-ESR measurements utilizing a custom-built heterodyne 128 GHz ESR spectrometer equipped with cryogenic mm-wave components and Fabry-Perot resonator (FPR). The sample was 50 μm-thick Si:P of the donor density of $6.52 \times 10^{16}\ cm^{-3}$, obtained by grinding a

piece of commercial wafer using a sandpaper. The sample was placed in the cavity of FPR which operates at TEM_{006} mode and frequency of 129.1 GHz and pressed by a thin (12um) Mylar film onto the flat mirror of the FPR as shown in Fig. 3.1. The flat mirror is made of 0.3 mm think sapphire disk with about 700 nm gold layer. Tuning the cavity was done without the sample at room temperature because strong absorption of mm-wave power by the sample made the resonance peak of the cavity to disappear. After tuning the empty cavity, the sample was placed inside the cavity and the temperature was lowered to 0.8 K. At low temperatures the resonance peak of the cavity reappeared because the Si:P sample became an insulator. The Q value of the cavity was about 3000. However, the presence of the sample made the cavity frequency to increase slightly from that of the empty cavity and thus be outside the optimum frequency range of the spectrometer (128-128.6 GHz). This led to a decrease of the excitation power and sensitivity of the spectrometer by factor 2-3. The maximum excitation field (B_1) is estimated to be about 1 mG. As increasing the attenuation level of the input attenuator, the excitation field decreases roughly as a square root of the attenuation level. A phase-locked Gunn oscillator was used as the mm-wave source having the excitation spectral width of 1.5 kHz. This value corresponds to the magnetic field resolution of better than 1 mG.

To obtain ESR spectrum of the sample, CW-ESR measurements were performed by sweeping the external magnetic field with the mm-wave frequency fixed. To sweep the magnetic field, two different sweep coils were used depending on measurement type. The main sweep coil, having the conversion factor between the magnetic field and the electrical current of about 61.3 G/A, is equipped with a persistent switch to vouch for negligibly small field drift during the measurements with the fine sweep coil (Fig. 3.2). The fine sweep coil, wound around the still radiation shield of the dilution refrigerator, has the conversion factor between the magnetic field and the electrical voltage of about 1.5 G/V. Because the maximum sweep width of the fine sweep coil is 30 G which is smaller than the hyperfine splitting of about 42 G in the ESR spectrum of the Si:P sample, it was impossible to get both hyperfine-split lines using the fine sweep coil. For this reason, so-called 'panorama' spectra were recorded using the main sweep coil. The two hyperfine-split lines in the ESR spectrum of the Si:P sample are labelled as 'L-line' for low field line and 'H-line' for the high field line. Each line is inhomogeneously broadened due to the presence of 29Si nuclei of the natural abundance (4.67%).

Hole burning measurements were performed by the following sequence. First set the magnetic field to the center of either L-line or H-line. Then

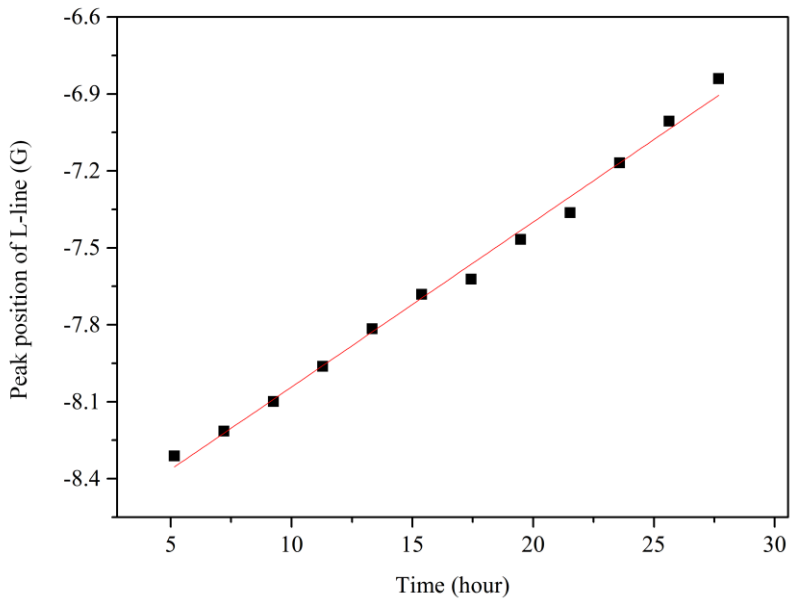

Figure 3.2: Field drift in a persistent mode of the main sweep coil. The peak position of L-line was recorded using the fine sweep coil. The linear fit gives the drift rate of about 65 mG/h.

decrease the attenuation level of the excitation mm-wave for a while. This is to burn a hole in an inhomogeneously broadened line. During this process, the depth of the burnt hole is measured to study the dynamics of burning hole. Afterward increase the attenuation level (stop burning) and measure ESR spectrum by sweeping the magnetic field to obtain the shape and its time dependence of the burnt hole. In this regard, it is important to avoid saturation effect, which spoils the shape of the burnt hole, by using small

enough excitation power during the measurement of the spectrum. We used the attenuation level of 30 dB and with this value no saturation effect was observed. From the obtained data of the hole shape and its time dependence, relevant dynamic nuclear polarization (DNP) and relaxation mechanisms were studied.

3.3 Results

ESR spectra measured at different temperatures are shown in Fig. 3.3. The spectrum of Si:P consists of three peaks, that is two hyperfine-split lines with about 42 G splitting and a central line between them. The background signals are due to unwanted paramagnetic material(s) inside the cavity. As temperature increases, overall signal amplitude decreases.

Fig. 3.4 shows an ESR spectrum after burning hole at the center of L-line for 3000 s with the highest excitation power, estimated to be hundreds of μW. The bulged peak right to the hole implies ^{29}Si DNP. Because the gyromagnetic ratio of ^{29}Si is negative, ^{29}Si DNP occurs toward high field, that is to say right side in the spectrum. On the other hand, the gyromagnetic ratio of ^{31}P is positive and thus ^{31}P occurs toward low field. This explains why there is no change on H-line after burning the L-line. Fig. 3.5 shows an ESR spectrum after burning hole at the center of H-line with

the same excitation condition. In H-line, a bulged peak appears at the right side of the hole, which implies ^{29}Si DNP. But this time, another bulged peak appears at L-line. This represents ^{31}P DNP [34]. Therefore burning hole at H-line generates DNP of both ^{31}P and ^{29}Si simultaneously. The relevant mechanism for the observed DNP is the Overhauser effect [35]. The effect relies on relaxation processes that simultaneously flip an electron spin and a nuclear spin which is often called cross relaxation. Fig. 3.6 and Fig. 3.7 show schematically cross relaxation processes for DNP of ^{31}P and ^{29}Si, respectively.

To study dynamics of DNP build-up, we measured the change of the depth of the burnt hole during high power excitation at L-line for different excitation powers (Fig. 3.8). It is clear that build-up of ^{29}Si DNP has a bi-exponential time dependence, which means that the DNP build-up is a two-step process. The short time constant may be related to the build-up of ^{29}Si DNP in the vicinity of donors. This is supported by the measured power dependence of the short time constant. As the excitation power increases, the short time constant increases. For high excitation power, the region of the vicinity of donors can be considered to be larger, and thus longer time is needed for fully polarizing ^{29}Si nuclear spins in the region because the rate of ^{29}Si DNP is limited by the rate of cross relaxation which is independent on

excitation power. Meanwhile the long time constant may be related to the ^{29}Si nuclear spin diffusion into region far from donors. The rate of the spin diffusion is determined by the strength of dipolar coupling between ^{29}Si nuclei and thus independent on excitation power. Note that at the highest excitation power (4 dB attenuation), the hole depth curve shows large drift during the measurement, which leads to large error on the long time constant.

Relaxation of ^{29}Si DNP was also studied. Fig. 3.9 shows time-dependent decay of hole depth after burning hole with various excitation conditions. For weak burning, i.e. 500 s with 30 dB attenuation and 20 s with 4 dB attenuation, the relaxation curves clearly show bi-exponential decay. Unfortunately, for other excitation conditions, the long time constant cannot be obtained reliably and thus it is hard to draw any conclusion on the dependence of relaxation mechanisms on excitation conditions. Further study will be needed to clarify relevant mechanisms.

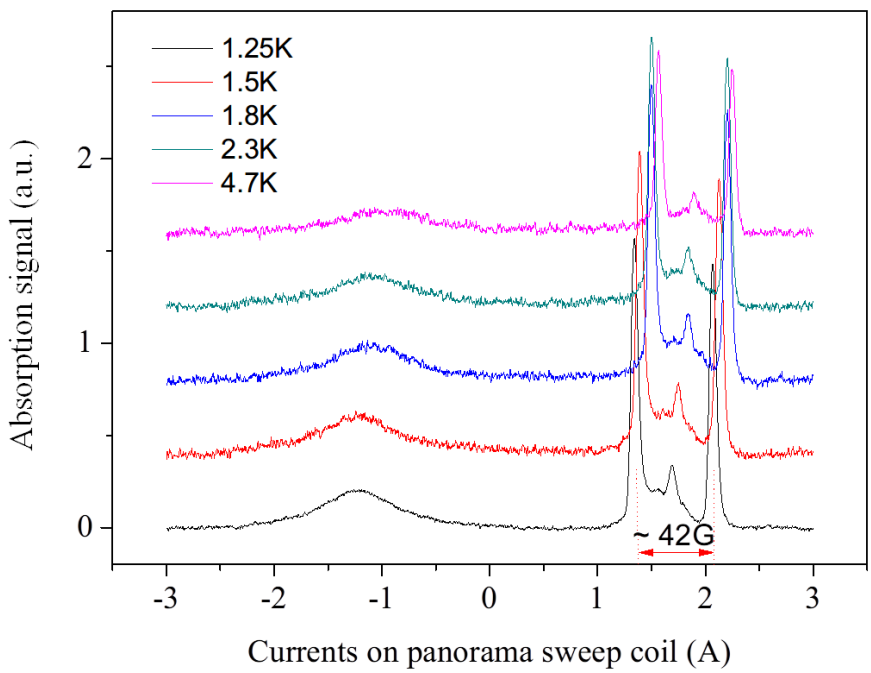

Figure 3.3: ESR spectra for Si:P ($\mathbf{6.52 \times 10^{16}}\ \boldsymbol{cm^{-3}}$) at different temperatures.

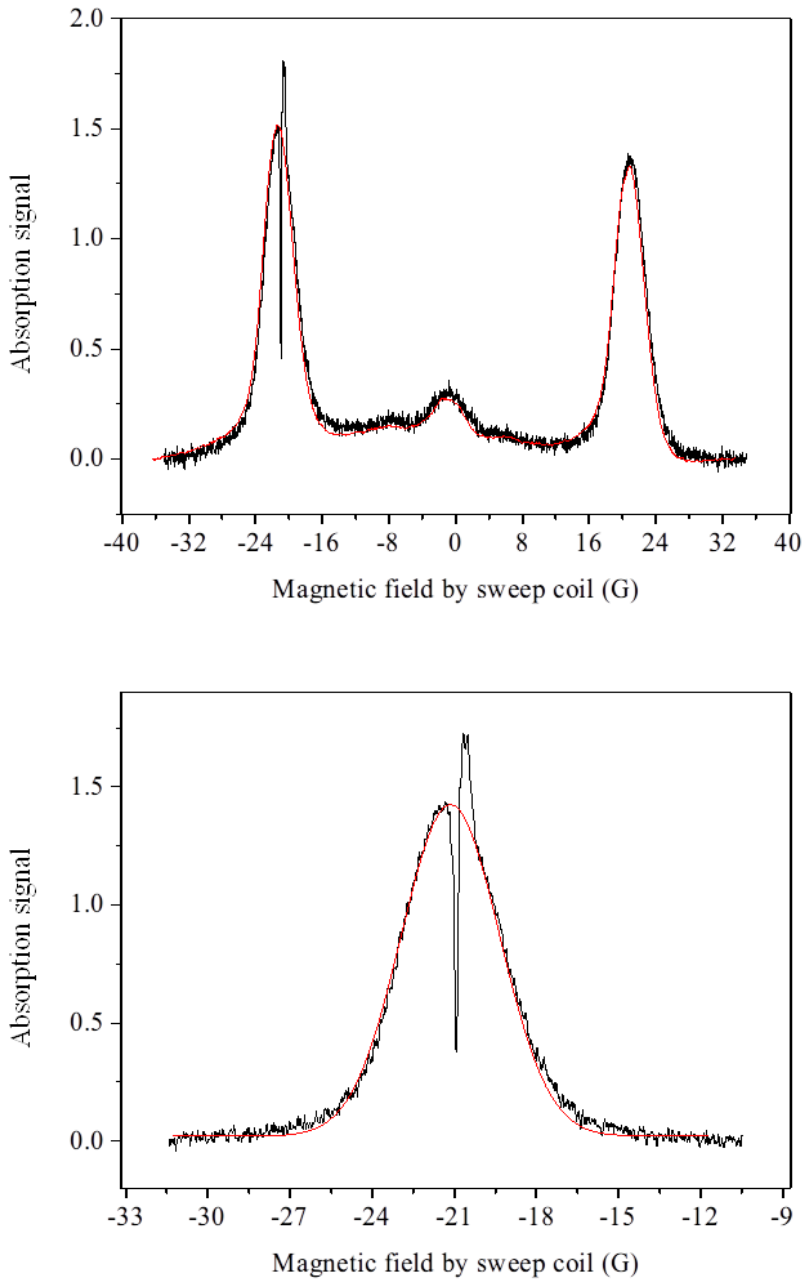

Figure 3.4: Burning hole on the low field line. The upper shows ESR spectrum of Si:P for after burning (black) and before burning (red). The bulged peak right to the hole implies DNP of ^{29}Si nuclei. The lower shows baseline-corrected low-field line.

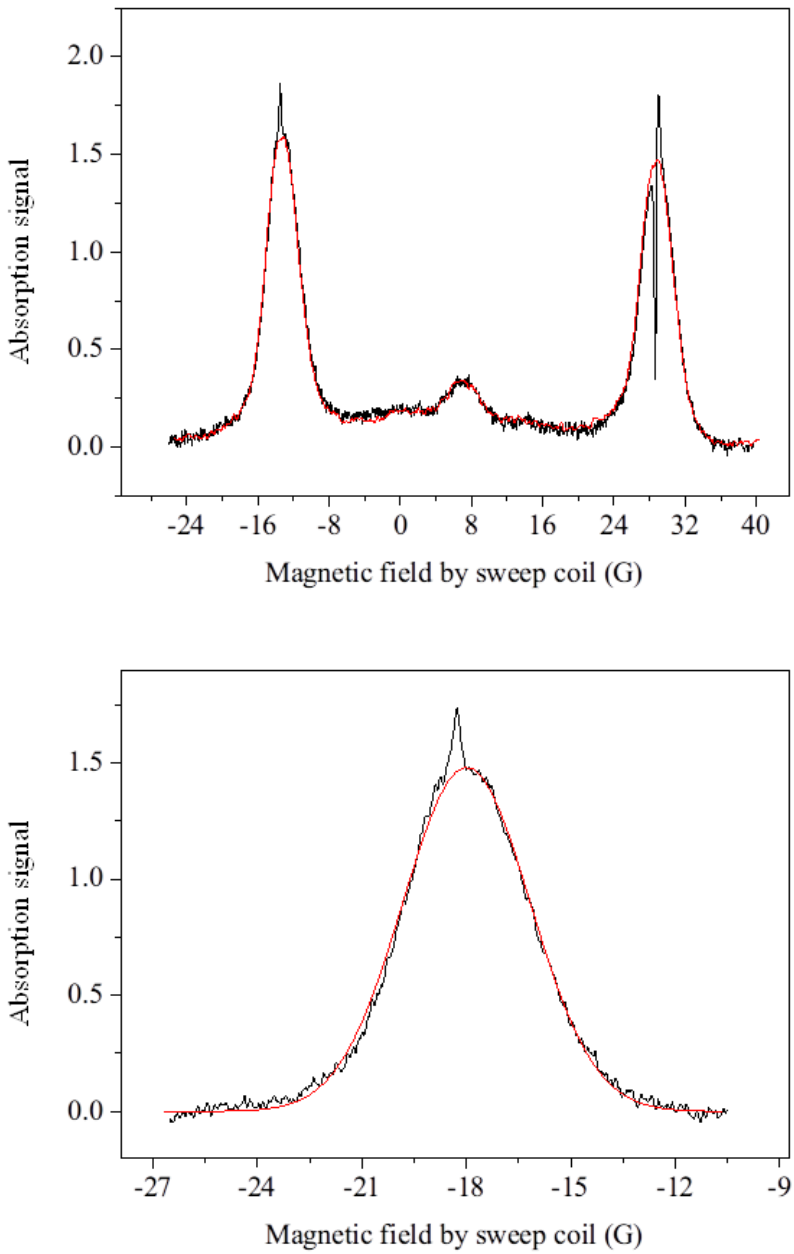

Figure 3.5: Burning hole on the high field line. The upper shows ESR spectrum of Si:P for after burning (black) and before burning (red). The bulged peak on the low field line implies DNP of ^{31}P nuclei. The lower shows baseline-corrected low-field line. ^{29}Si DNP is also shown at the high field line.

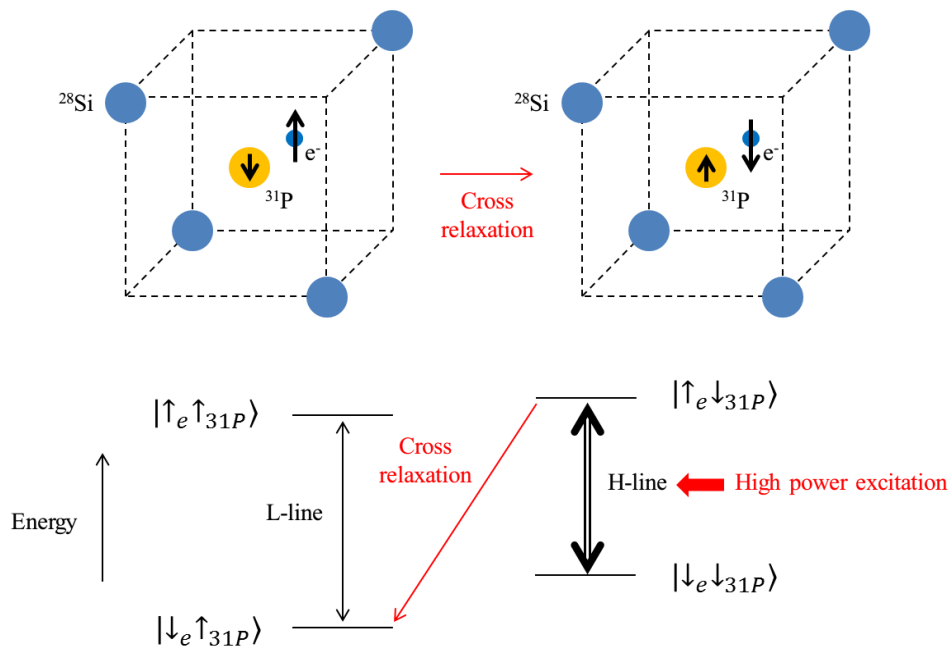

Figure 3.6: Mechanism for ^{31}P DNP by the Overhauser effect. Cross relaxation, by which an electron spin and a ^{31}P nuclear spin make a mutual spin flip−flop, leads to enhancement of the ^{31}P nuclear polarization. Here the high power excitation it to saturate the high field ESR line (H−line).

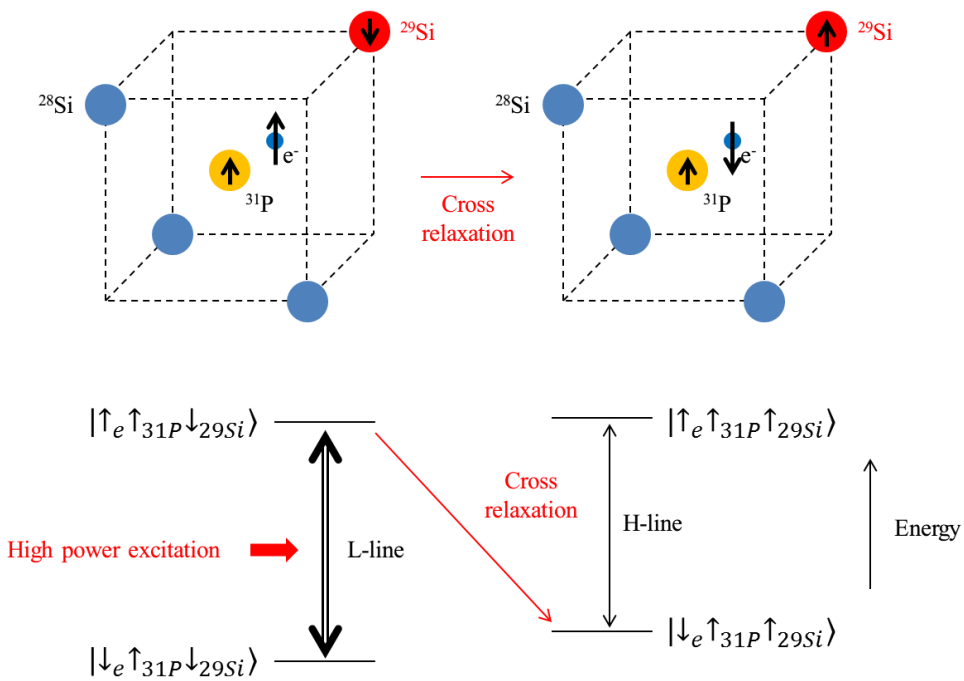

Figure 3.7: Mechanism for ^{29}Si DNP by the Overhauser effect. Cross relaxation, by which an electron spin and a ^{29}Si nuclear spin make a mutual spin flip–flop, leads to enhancement of the ^{29}Si nuclear polarization. Here the high power excitation it to saturate the low field ESR line (L–line).

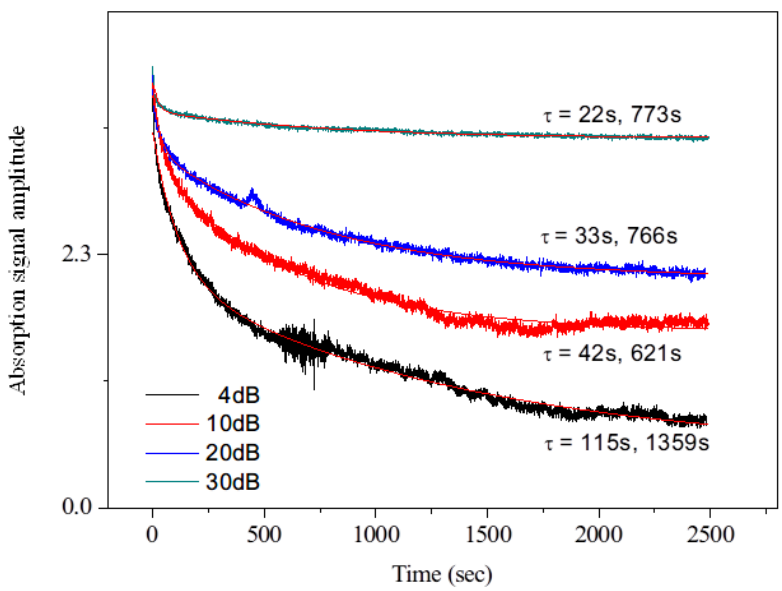

Figure 3.8: Dynamics of burning hole on the low-field line for different of excitation powers. The 4 dB attenuation (black) corresponds to the maximum excitation power. Bi-exponential fit curves (red) are also shown with the obtained time constants.

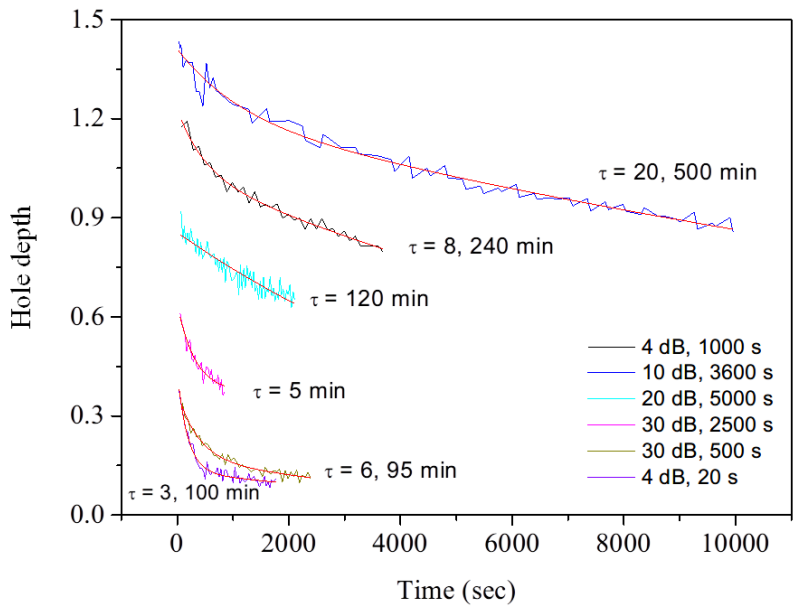

Figure 3.9: Relaxation of the hole after burning hole on the low field line for different excitation conditions. The legend shows corresponding attenuations and excitation times. Bi−exponential fit curves (red) are also shown with the obtained times constants.

Chapter 4

Relaxation of Donor Electrons in Si:P

4.1 Overview

In this chapter, experimental results of relaxation times in Si:P will be presented. The pulsed ESR experiment was performed at Korea Basic Science Institute, Daejeon, Korea. The relaxation times of Si:P with the donor density high enough for the exchange coupling between donor electrons to be important, were measured. Regarding transverse relaxation, the dominant decoherence mechanisms turned out to be instantaneous diffusion and spectral diffusion. Detailed discussions on both mechanisms will be given.

4.2 Experimental details

Pulsed ESR experiments were performed using a Bruker's W-band (75-110 GHz) ESR spectrometer (Elexsys E680) equipped with a standard resonator (EN 680-1021H). A picture of the system is shown in Fig. 4.1.

Figure 4.1: Picture of the Bruker W-band ESR system (Elexsys E680)

The resonator has a cylindrical cavity which operates at TE_{011} mode and the frequency around 94 GHz (Fig. 4.2). The system features a superheterodyne spectrometer which utilizes intermediate frequency (IF) from 9 to 10 GHz for highly sensitive detection. The schematic diagram of the W-band microwave bridge is shown in Fig. 4.3. The local oscillator supplies microwave power at the frequency of 84.5000 GHz with an accuracy better than 100 kHz with the aid of the phase lock circuit. Then the upconverter mixes the 84.5 GHz from the local oscillator and the IF frequency from the IF bridge to generate the excitation frequency around 94 GHz. Then the

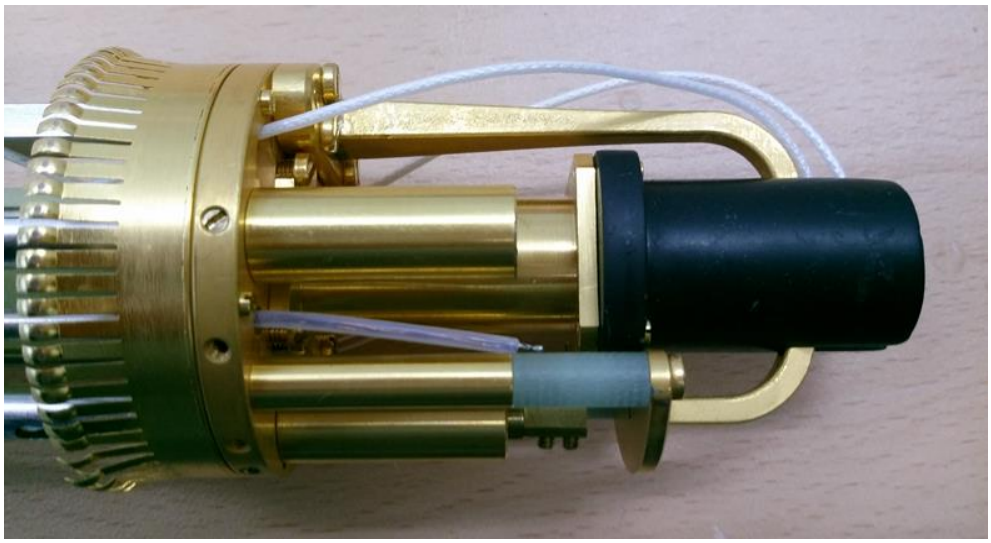

Figure 4.2: Picture of the ESR resonator (EN 680-1021H).

ESR signal from a sample in the resonator goes to the downconverter through the circulator. Finally the signal is amplified by the low noise amplifier and sent to the IF bridge. In the IF bridge, the signal is processed depending on measurement type to render raw data. The experimental temperature of 4 K was obtained by a dynamic continuous flow cryostat (Oxford CF935) and a temperature controller (Oxford ITC 503).

Samples with two different donor densities were used for relaxation measurements. To be inserted into the standard sample tube with 0.5 mm inner diameter, small pieces of Si:P single crystal were detached from commercial wafers of Virginia Semiconductor Inc. with different donor

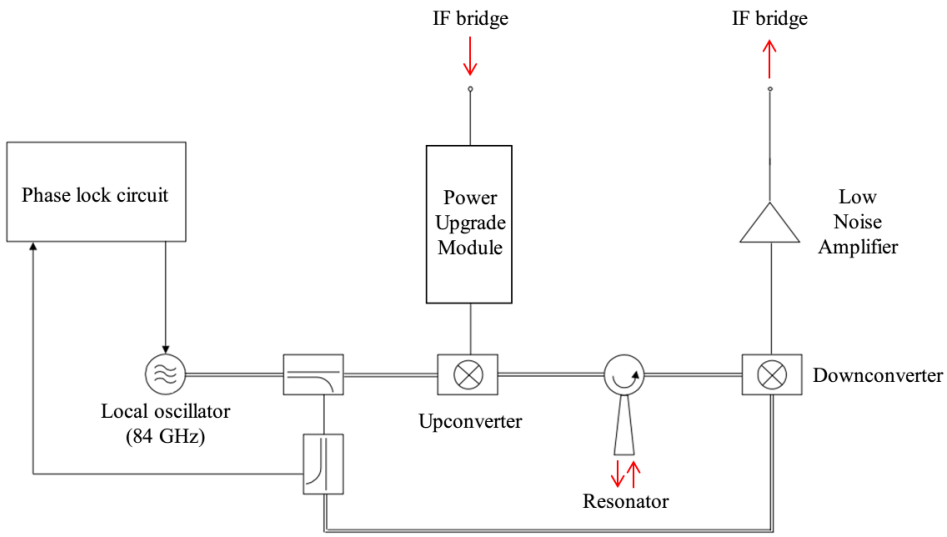

Figure 4.3: Schematic diagram of the W-band bridge.

densities of $6.52 \times 10^{16}\ \mathrm{P \cdot cm^{-3}}$ and $1.1 \times 10^{17}\ \mathrm{P \cdot cm^{-3}}$.

With the aid of Bruker's 100 mW W-band power upgrade module, 90° and 180° pulses of 14 and 28 ns were used, respectively. The length of each pulse was determined by a transient nutation measurement with pulse sequence $(\theta - T - \frac{\pi}{2} - \tau - \pi - \tau - \mathrm{echo})$, where θ is the varying tipping angle of the first pulse, and T and τ are fixed delays between pulses (Fig. 4.4). From the obtained length of about $56\ \mathrm{ns}$ for the 2π-pulse, the length of the $\frac{\pi}{2}$-pulse and π-pulse was confirmed to be 14 ns and 28 ns, respectively. The obtained value of the π-pulse length corresponds to the B_1

field magnitude of about 18 MHz. For the electron paramagnetic resonance spectrum of the phosphorus doped silicon, it is well known that the width of each inhomogeneously broadened line is about 2.5 G [7]. This corresponds to the offset field of about 7 MHz, considering the gyromagnetic ratio of the free electron (28 GHz/T). Because the B_1 field is larger than the offset field, it is safe to say that the pulses nonselectively excite one of the hyperfine split lines. This is confirmed by the Fourier transform of the measured echo signal in the time domain shown in Fig. 4.5.

For the sample with $6.52 \times 10^{16}\ P \cdot cm^{-3}$, echo detected field swept spectrum was measured at the temperature of 5 K and the external magnetic field of about 3.4 T. The measurement was performed using the Hahn echo sequence $(\frac{\pi}{2} - \tau - \pi - \tau - echo)$ to obtain the integration of echo signal in the real channel of the quadrature receiver while sweeping the magnetic field. Based on the obtained spectrum, the longitudinal relaxation time was measured at different temperatures of 4–22 K using the inversion recovery pulse sequence $(\pi - T - \frac{\pi}{2} - \tau - \pi - \tau - echo)$, where T is the varying delay during which thermal contact with the lattice takes place. Also the transverse relaxation time was measured at the same temperature range using the Hahn echo sequence. However, when the intervals between pulses in the sequence are longer than several μsec, unusual fluctuations arose in

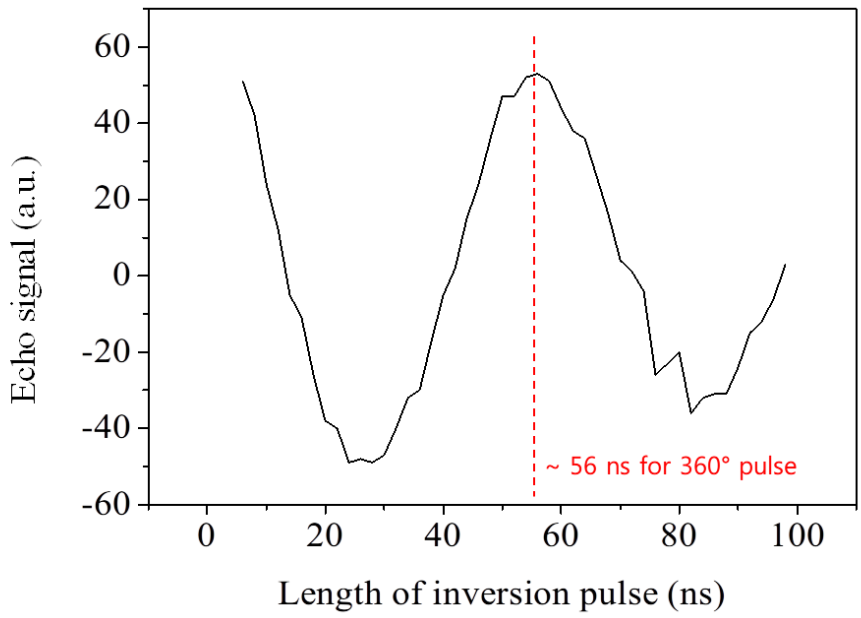

Figure 4.4: Rabi oscillation by the nutation measurement. Donor density was $\mathbf{1.1 \times 10^{17}}\ \boldsymbol{cm^{-3}}$, temperature 4 K.

the echo phases. This is the instrumental phase noise reported by Tyryshkin and et al. [36]; it is considered to be due to fluctuations of the external magnetic field or phase instability of the microwave source. With state-of-the-art electron spin resonance equipment, it appears to be difficult to solve this problem completely.

To overcome the instrumental phase noise in a roundabout way, we followed Tyryshikin's method: 2D signal from a quadrature receiver are

combined to yield the magnitude of echo, and then average the magnitude data. For repeating measurements with this magnitude-average method, a home-built code was used with Bruker's macro programming language (PRODEL) (Fig. 4.6). Each data point in echo decay curves was obtained by the average of 10 data instances from the magnitude-average method. This works well for the Hahn echo sequence. However, for dynamical decoupling measurements presented in Chap. 5, the use of multiple π-pulses makes the situation worse. This will be discussed in Chap. 5 in detail.

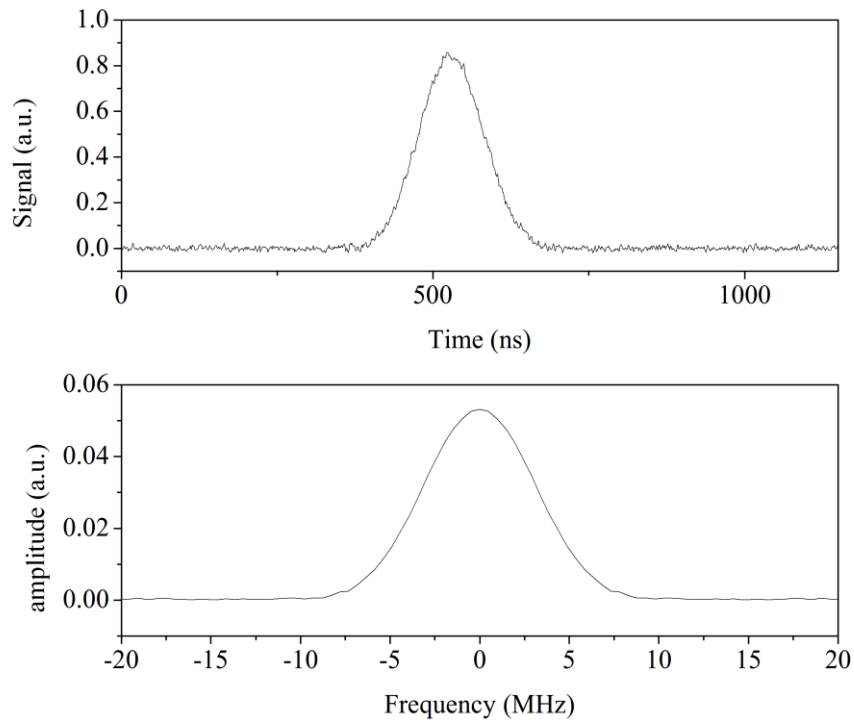

Figure 4.5: Echo signal in the time domain and its Fourier transform. Donor density was $\mathbf{1.1 \times 10^{17}\ cm^{-3}}$, temperature 4 K. The FWHM of the spectrum is about 2.5 G.

4.3 Results

An echo detected field swept spectrum of the Si:P sample with the donor density of $7 \times 10^{16}\ cm^{-3}$ at the temperature of 5 K is shown in Fig. 4.7. The splitting between two lines is about 42 G which corresponds to the hyperfine interaction between electron and ^{31}P nucleus. The center line, which was observed by CW-ESR measurement in Chap. 3, does not appear here because it is homogeneously broadened and thus does not contribute echo signal. The large difference between amplitudes of hyperfine-split lines may be due to imperfect echo phase at H-line because receiver phase was set to maximize the real channel signal at L-line. It is worth to check if the difference arises from the ^{31}P nuclear polarization. Because the gyromagnetic ratio of ^{31}P nuclei is about 17.2 MHz/T, its Zeeman splitting in the external magnetic field of 3.4 T is about 58 MHz. Considering the temperature of 5 K corresponds to about 104 GHz in frequency dimension, ^{31}P populations at both spin states are almost same ($\exp\left(-\frac{0.058}{104}\right) \cong 0.999$). Thus ^{31}P nuclear polarization does not contribute to the observed difference in peak amplitudes.

The measured longitudinal relaxation times for L-line of the sample with $7 \times 10^{16}\ P \cdot cm^{-3}$ are shown in Fig. 4.8. The measured temperature

dependence of longitudinal relaxation time T_1 can be well fit by the known empirical formula of $y = aB^4T + bB^2T^7 + cexp\left(-\frac{d}{T}\right)$ [37], [38]. In this equation, the first term corresponds to the direct phonon process by which excited electron spin loses its energy to lattice while creating a phonon. On the other hand, the second and third terms are due to the Raman process and the Orbach process [39], respectively. These processes concern two phonons for the relaxation of electron spin. The obtained fitting parameters with the constraint of $\mathrm{B} = 3.36\,\mathrm{T}$ are as follows: $\mathrm{a} = 3.73 \times 10^{-3}\ (\pm 9 \times 10^{-5})\ \mathrm{T^{-4}K^{-1}s^{-1}}$, $\mathrm{b} = 1.48 \times 10^{-7}\ (\pm 3.1 \times 10^{-8})\ \mathrm{T^{-2}K^{-7}s^{-1}}$, $\mathrm{c} = 6.21 \times 10^{8}\ (\pm 2.0 \times 10^{7})\ \mathrm{s^{-1}}$, $\mathrm{d} = 1.37 \times 10^{2}\ (\pm 4 \times 10^{-1})\ \mathrm{K}$. Our results show that the dominant mechanism for the longitudinal relaxation in the given experimental condition is the direct phonon process at temperatures lower than 7 K, while the Orbach process is dominant at temperatures higher than 7 K. This agrees with the previous results for high magnetic fields [37], [36].

The measured transverse relaxation times for the same experimental condition are shown in Fig. 4.9. Here the T_1 fit curve obtained in Fig. 4.8 is also shown because comparison of T_1 and T_2 has important meaning on measurements of relaxation times. At temperatures higher than 11 K, the measured echo signal shows single exponential decay and the relevant time constant T_2 is coincident with T_1. This implies that, at high temperatures, the

transverse relaxation is dominated by the longitudinal relaxation. On the other hand, at temperatures lower than 11 K, T_1 becomes much longer than T_2 and the echo decay shows an additional decay factor of compressed exponential form. The time constant of the compressed exponential decay is often called T_{sd} named after the relevant mechanism, spectral diffusion. Both T_2 and T_{sd} show no temperature dependence at low temperatures. This is as expected because both time constants are determined by dipolar interactions between spins which is independent on temperature.

To study mechanisms relevant to the measured time constants in detail, Hahn echo decay for the sample with $1.1 \times 10^{17}\ \mathrm{P \cdot cm^{-3}}$ was measured at 4 K (Fig. 4.10). Note that, from the result of Fig. 4.9, it is clear that longitudinal relaxation does not contribute to echo decay at 4 K. In Fig. 4.10, The measured (normalized) echo decay has the form of $E(2\tau) = \exp\left\{-\frac{2\tau}{T_2} - \left(\frac{2\tau}{T_{SD}}\right)^n\right\}$. The exponential factor (red dotted line) was obtained from the UDD7 data presented in Chap. 5. Using this result ($T_2 = 0.9\ \mathrm{ms}$) as a constraint, the fitting was performed to obtain T_{SD} of about 0.26 ms and n of about 2.7. Further discussion on these values, related to spectral diffusion, will be given in the Section 4.5.

We first focus on mechanisms responsible for the single exponential decay factor (T_2). In principle, transverse relaxation is the manifestation of

decoherence of spins. Electron spin decoherence in silicon has been studied intensively over decades, and researchers have revealed the relevant decoherence mechanisms, and their dependence on temperature and the density of impurities [5], [7], [40]. At low temperatures, where the effect of the interaction with the thermal bath of lattice phonons is negligible, the decoherence of electron spins in isotopically-purified silicon with almost no ^{29}Si impurities, is governed by the dipolar interaction between electron spins [40], [10]. Let's consider the decoherence of an electron spin surrounded by other donor electrons in the presence of the external magnetic field which is strong enough to render a good quantization axis for the electron spins. Then the effects of the dipolar interaction between the central spin and one of the neighbors on the decoherence can be understood in terms of the dipolar field produced by the neighboring spin. The longitudinal component (parallel to the external field) of the dipolar field contributes to the Larmor precession frequency of the central spin. Thus, if the neighboring spin fluctuates with time for some reason, the initial coherent state of the central spin becomes untraceable, that is, decoherence occurs. One way to achieve such spin fluctuation is an applied microwave pulse, which rotates all resonant electron spins (Fig. 4.11). This mechanism, often called instantaneous diffusion [40], [41], is an artificial effect due to ensemble

measurements. Meanwhile, the transverse component (perpendicular to the external field) of the dipolar field induces a flip of the central spin together with a flop of the neighboring spin as an expression of energy conservation. This direct flip-flop leads to the complete decoherence of the central spin (Fig. 4.12).

Both instantaneous diffusion and direct flip-flop result in single exponential decay of echo amplitude. If we define $\frac{1}{T_{ID}}, \frac{1}{T_{DF}}$ as the decoherence rates due to the instantaneous diffusion and the direct flip-flop, respectively, then $T_2 = \frac{T_{ID}T_{DF}}{T_{ID}+T_{DF}}$. In our sample which is isotopically natural, the presence of ^{29}Si introduces inhomogeneous broadening of ESR lines. Because the rate of the flip-flop of electrons, which leads to direct flip-flop process, is inversely proportional to the inhomogeneous line width [42], it is expected that T_{DF} becomes longer due to ^{29}Si nuclei. The estimated of T_{DF} for our sample is about a second. The estimation is based on the previous results which confirmed that the inhomogeneous line width for isotopically natural silicon is larger than that of isotopically purified silicon with residual ^{29}Si impurities of only $50\ \mathrm{ppm}$ by three orders of magnitude [3], [43]. From the result of Tyryshkin et al. [40], T_{DF} of $0.8\ (\pm 0.15)\ \mathrm{s}$, for such extremely purified silicon (donor density of $1.2 \times 10^{14}\ /\mathrm{cc}$), T_{DF} for our sample with $1.1 \times 10^{17}\ \mathrm{P/cc}$ can be estimated to be a similar value because the rate of

the electron-induced spectral diffusion, $1/T_{SD}$, scales with the donor density. Because the estimated T_{DF} is larger than the measured T_2 of 0.9 ms by three orders of magnitude, we can safely ignore the contribution of T_{DF} to T_2, that is, the contribution of instantaneous diffusion (T_{ID}) is dominant. In the next section, detailed discussion on instantaneous diffusion will be presented.

```
# Experiment for T2 measurements (Hahn echo)#
# Dec 2013 #
# by Minchan Gwak #

program T2_Hahn_Raw(int ExpDate; int NoOfPoints;
int Init_Tau_ns; int Tau_Step_ns; int NoOfAverage);

# Declaration of variables #
int       i, j, k, n, m, l, p, tau_step, DsetHandle,
dim[8], d[8];
real      yr[1024], yi[1024], x[256];
pointer   CurExp, CurExpName, Dset;
boolean   ;
char      s[100],   DsetTitle[100],   Directory[300],
Date[100];

while (i < 8)
          dim[i] = 0;
          i = i + 1;
endwhile;

# Variables for experimental parameters #

strcpy(Date, ExpDate);
n = NoOfPoints;
tau_step = Tau_Step_ns;
l = NoOfAverage;

# Set pointer variables for experiment #
CurExp = aqGetSelectedExp(-1);
  # get a reference to the experiment selected in the
current viewport #
if (CurExp == NIL)
          printLn("No experiment has been selected
for current viewport");
          return(FALSE);
endif;
CurExpName = aqGetExpName(CurExp);

# Activate experiment #
  # (not needed because it would be already
activated) #
  # aqExpActivate(CurExp); #

# Set an experimental parameter to the value it
should be #
execCmd("aqParSet",                    CurExpName,
""*ftEpr.PlsSPELSetVar' 'h=1"");
#          execCmd("aqParSet          'AcqHidden'
'*specJet.TimeBase' '1""); #


# Measurement #

printLn("Hahn Echo Pulse sequence : (90-d1-180-d1-
echo)");
printLn("Progress : ", n, " * ", l);

k = 0;
while (k < l)
  d[1] = Init_Tau_ns;
  i = 0;
  while (i < n)
    print(i, " ");
    d[2] = d[1]*2;
    x[i] = d[2];
    execCmd("aqParSet",              CurExpName,
""*ftEpr.PlsSPELSetVar' 'd1=", d[1], """);
    aqSetSelectedExp(1, CurExpName);
    aqExpRunAndWait(CurExp);
    Dset = getCopyOfPrimary;

    strcpy(DsetTitle,
"SiP_Crystal(small)_T2_Hahn_4K_");
    strcat(DsetTitle, "d1_");
    strcat(DsetTitle, d[1]);
    strcat(DsetTitle, "ns_");
    strcat(DsetTitle, k+1);
    setTitle(Dset, DsetTitle);
    DsetHandle = storeCopyOfDset(Dset);
    execCmd("ddSecurity all just_do confirm no
yes");
    execCmd("vpCurrent Primary ",DsetHandle);
    execCmd("ddCurrent", DsetHandle);
    strcpy(Directory,
"/home/xuser/xeprFiles/Data/E1930/Minchan/SiP/");
    strcat(Directory, Date);
    strcat(Directory, "/");
    strcat(Directory, DsetTitle);
    strcat(Directory, ".dat");
    execCmd("ddSaveAsc -1", Directory);
    execCmd("ddRemove -1");

    d[1] = d[1] + tau_step;
    i = i + 1;
  endwhile;

  printLn("");
  printLn(k);
  k = k + 1;
endwhile;

goto FinalDataProcessing;


label FinalDataProcessing;
aqSetSelectedExp(1, CurExpName);
return(TRUE);

label ERROR;
printLn("An error(s) happened.");
return(TRUE);
```

Figure 4.6: A home-built code of PRODEL for Hahn echo measurement in the presence of instrumental phase noise.

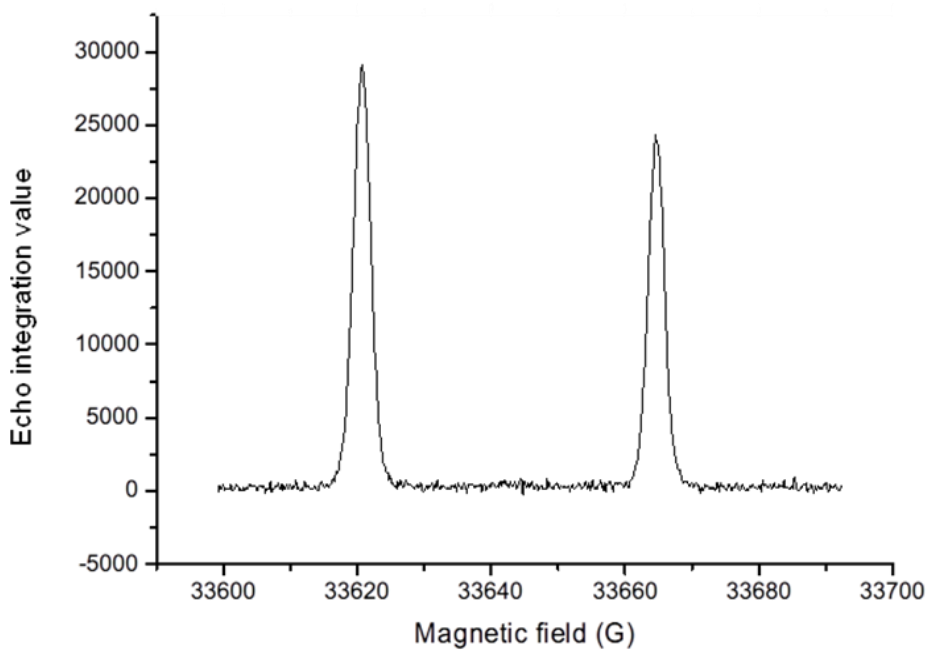

Figure 4.7: Echo detected field swept spectrum of Si:P at 5 K. The sample has the donor density of $\mathbf{6.52 \times 10^{16}\ cm^{-3}}$.

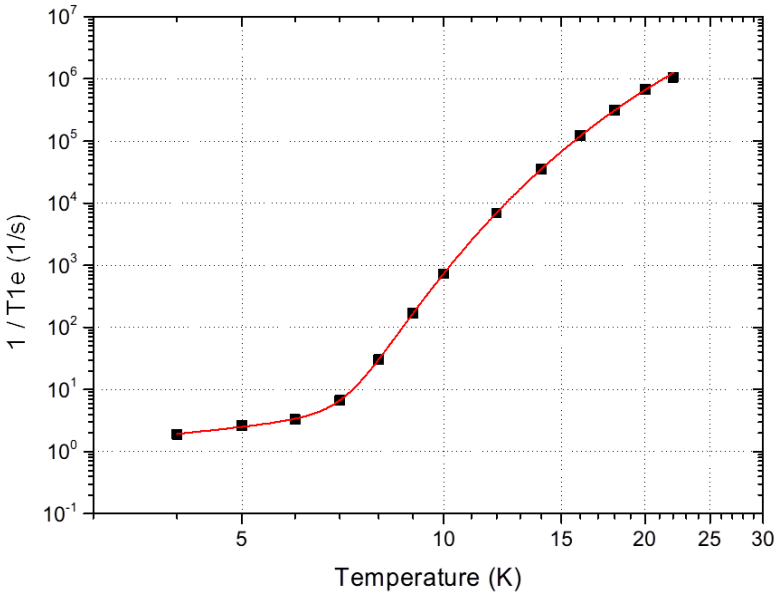

Figure 4.8: Temperature dependence of longitudinal relaxation time for the sample with $\mathbf{6.52 \times 10^{16}}\ \boldsymbol{P \cdot cm^{-3}}$. The conventional inversion recovery pulse sequence was used. The fit curve (red) represents the empirical formula, $\boldsymbol{y = aB^4T + bB^2T^7 + cexp\left(-\frac{d}{T}\right)}$, where $\boldsymbol{B}$ is the external magnetic field (3.36 T in this case) [37].

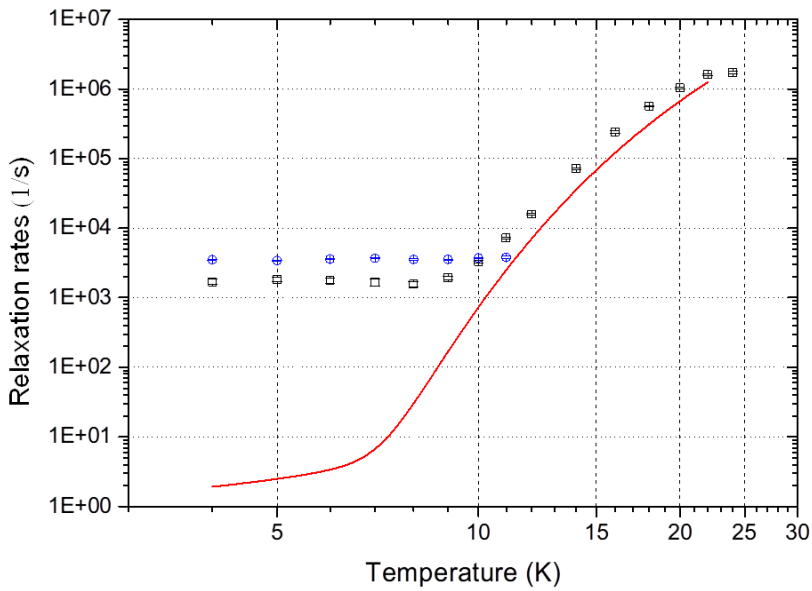

Figure 4.9: Temperature dependence of transverse relaxation time for the sample of $\mathbf{6.52 \times 10^{16}}\ \boldsymbol{P \cdot cm^{-3}}$. Below about 11 K, echo decay curves have a product form of single exponential decay and compressed exponential decay. Time constants for each decay factor are represented as square (single exponential) and circle (compressed exponential). The red line is the fit curve to the longitudinal relaxation times in Fig. 4.8.

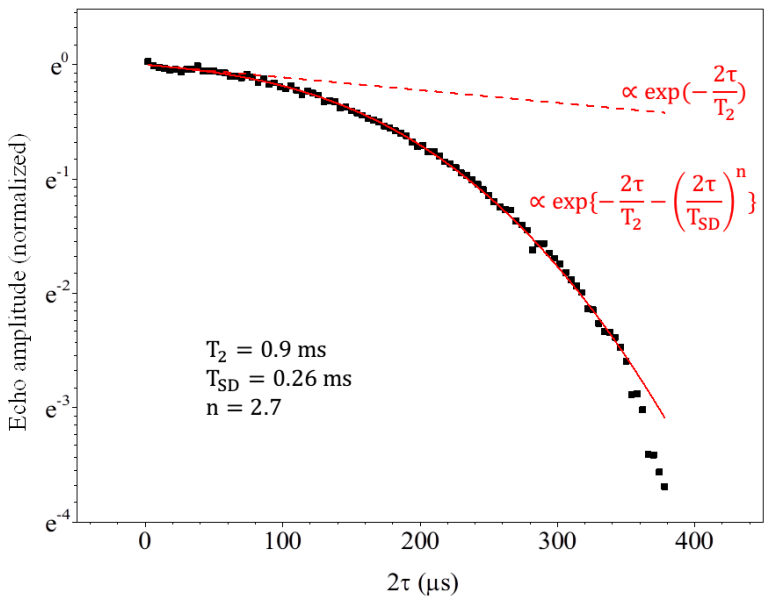

Figure 4.10: Electron spin echo decay for isotopically natural silicon with the donor density of $\mathbf{1.1 \times 10^{17}\ P/cm^3}$ at 4 K by the two−pulse Hahn echo sequence $(\frac{\pi}{2} - \tau - \pi - \tau - \mathbf{echo})$. The measured (normalized) echo decay has the form of $\mathbf{E(2\tau) = exp\left\{-\frac{2\tau}{T_2} - \left(\frac{2\tau}{T_{SD}}\right)^n\right\}}$. Red curve represents the fit curve. The exponential factor is shown separately (red dotted line).

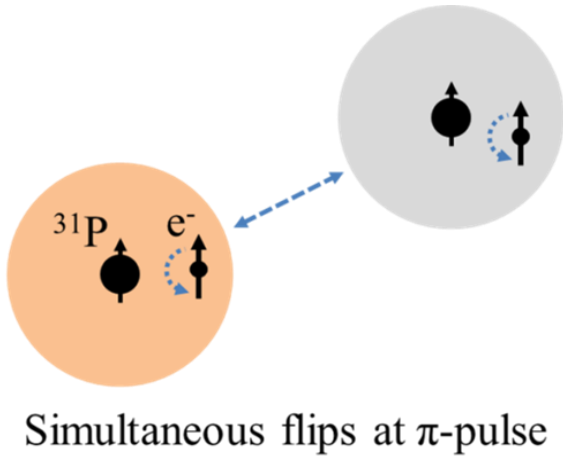

Figure 4.11: Diagram for the mechanism of instantaneous diffusion. Pulse-induced flip of neighboring electron spin (grey) leads to the fluctuation of the local magnetic at a central spin (red).

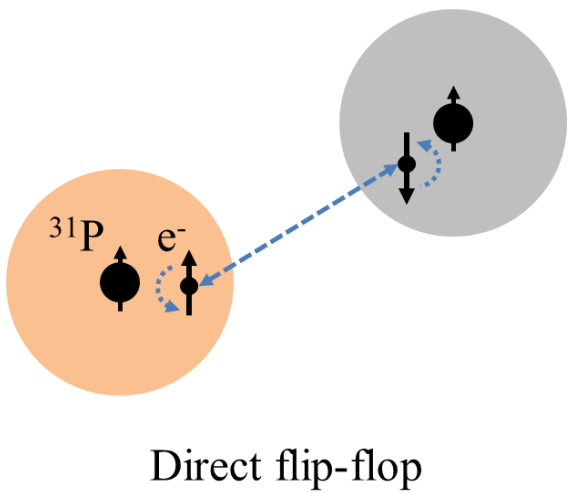

Figure 4.12: Diagram for the mechanism of direct flip-flop. Dipolar coupling between electron spins leads to a mutual flip-flop.

4.4 Instantaneous diffusion

As shown in the previous section, the measured T_2 of about 0.9 ms can be thought as T_{ID}. However this value is much larger than the theoretically estimated value of about 0.02 ms [6]. For this estimation, the equation which had been derived for low donor densities was used:

$$\frac{1}{T_{ID}} = C\pi\mu g^2 \mu_B^2 \sin^2\left(\frac{\beta}{2}\right)/(9\sqrt{3}\,\hbar), \tag{4.1}$$

where C is the concentration of the resonant electron spins ($C = \frac{1}{2}[P]$ for the donor density $[P]$ in our case), μ is the permeability of crystalline silicon, g is the g-factor of the donor electron, μ_B is the Bohr magneton and β is the tipping angle of the refocusing pulse. The large discrepancy can be explained by the presence of exchange-coupled donor pairs. As shown in Chap. 2, as the donor density increases, the number of exchange-coupled donor pairs also increases. For example, for the donor density of $1 \times 10^{17}\ /cc$, about 60 % of donor pairs have the exchange constant J larger than electron Larmor frequency for the donor density of $1 \times 10^{17}\ /cc$ in the presence of magnetic field of 3.4 T [44]. Because most of these donor pairs with strong exchange coupling reside in the singlet state ($S = 0$) which is irrelevant to ESR, an ESR-effective donor density, or C will be smaller than $\frac{1}{2}[P]$. This can explain qualitatively the increase of the measured T_{ID} compared to the

theoretical value. However more rigorous analysis will need measurements for various donor densities. From the eq. (4.1), it can be seen that T_{ID} also depends on the tipping angle β of the refocusing pulse in echo sequence. Thus an infinitesimally small tipping angle for the refocusing pulse is used, instantaneous diffusion will become negligible. However echo signal intensity decreases with the decrease of the tipping angle, so we used an extrapolation method [6], [40], [45] from the measured T_2 data for different tipping angles (Fig. 4.13). It is expected that the extrapolation to $\beta = 0$ will give time constant regarding electron-induced spectral diffusion (see Section 4.5), but unfortunately, poor SNR makes it difficult to extract reliable fitting parameters.

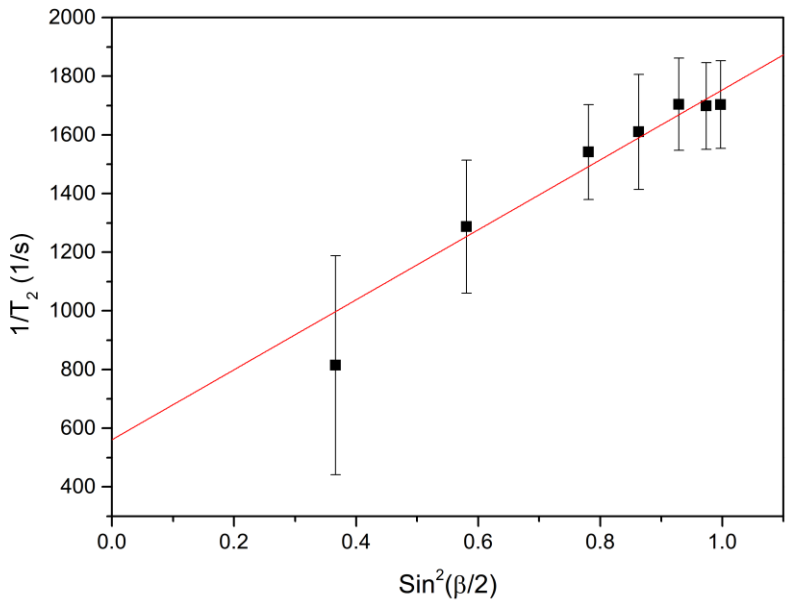

Figure 4.13: Suppression of instantaneous diffusion by decreasing the tip angle (**β**) of the refocusing pulse in the Hahn echo sequence. Black dots represent the measured relaxation time for instantaneous diffusion.

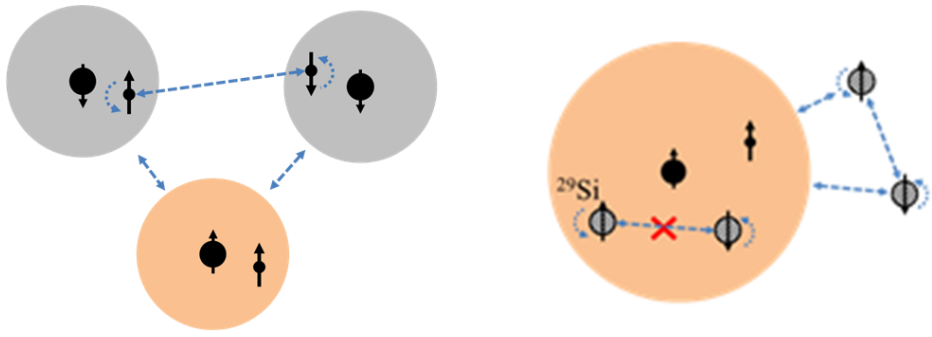

Flip-flop of nearby electron spins

Flip-flop of nearby nuclear spins

Figure 4.14: Diagram for the mechanism of spectral diffusion. Dipolar interaction between spins induces mutual flip-flip of spins which results in the fluctuation of the local magnetic field at a central spin (red). The left figure shows flip-flop of nearby electron spins and the right figure flip-flop of nearby ^{29}Si nuclear spins.

4.5 Spectral diffusion

The measured T_{SD} is related with often called spectral diffusion process. In the same way as direct flip-flop, dipolar interaction between donor electrons also leads to flip-flops of electron spins neighboring to a central spin (Fig. 4.14). This results in time-dependent fluctuation of the local magnetic field at a central spin and thus the refocusing of the net magnetization by π-pulse becomes imperfect. Meanwhile, ^{29}Si nuclei are also coupled to each other by dipolar interaction and thus they can make

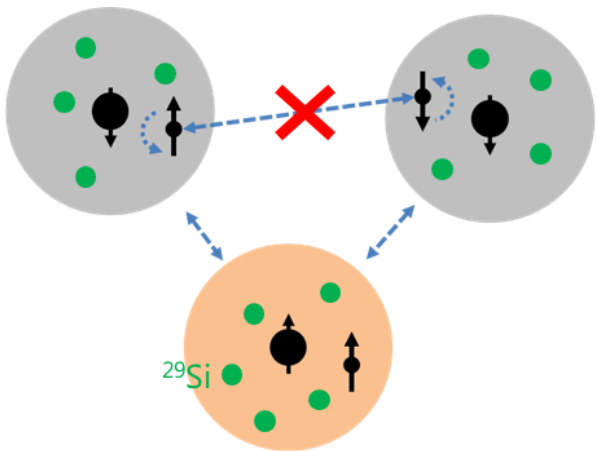

Figure 4.15: The suppression of electron-induced spectral diffusion by the presence of ^{29}Si nuclei.

flip-flops (Fig. 4.14) which leads to decoherence of a central spin. These mechanisms regarding time-dependent random fluctuation of local magnetic field are called spectral diffusion.

As described in Section 4.3, the presence of ^{29}Si nuclei suppresses direct flip-flop process by inducing inhomogeneity on electron Larmor frequencies. Naturally, the same way can be applied to electron-induced spectral diffusion which concerns flip-flops of donor electrons. That is to say, the inhomogeneous magnetic field due to randomly distributed ^{29}Si nuclei prevents the flip-flop of electron spins (Fig. 4.15). From the result of Tyryshkin et al. [40] of T_{SD} of $1.3(\pm 0.1)$ s for an extremely purified silicon

(donor density of $1.2 \times 10^{14}\ /cc$), the suppressed electron-induced spectral diffusion in our sample is considered to have a similar value. Thus contribution of the electron-induced spectral diffusion to the measured T_{SD} of about 0.26 ms can be thought as negligible. This is also confirmed by the fact that the measured T_{SD} is in agreement with the result of Abe et al. [43] for isotopically natural silicon with phosphorus donor density of about $10^{15}\ /cc$ which is low enough to ignore the electron-induced spectral diffusion. Therefore, our result shows that the (^{29}Si) nuclear-induced spectral diffusion is still dominant in our sample, even with a much higher donor density ($\sim 10^{17}\ /cc$).

It is worth considering the meaning of the measured $T_{SD}(= 0.26\ ms)$ and $n\ (= 2.7)$ regarding the prospect of fault-tolerant quantum computation. Assuming that the instantaneous diffusion and the direct flip-flop are negligible, the electron spin coherence decays in the form of $\exp\{-\left(\frac{t}{T_{SD}}\right)^{n}\}$, as described above, and the error probability is given as $[1 - \exp\{-\left(\frac{t}{T_{SD}}\right)^{n}\}]$; where t is the total free-precession time and corresponds to 2τ in the Hahn echo sequence. According to Preskil's estimation[46] on fault-tolerant CNOT operation with quantum computers, the error probability per qubit operation should be lower than 10^{-5}. Using the above equation for the

error probability, and the measured values of T_{SD} and n, the total free-precession time t, which corresponds to the error probability of 10^{-5}, is found to be about $3.7\,\mu s$. This time sets an upper bound on the qubit operation time. If we try to implement a microsecond qubit operation, one significant obstacle is the error of the gating pulse length because it directly contributes to the error of the qubit operation. To satisfy the error threshold of 10^{-5}, the gating pulse length should be controllable with ten picosecond accuracy, which is far beyond currently available pulse-generation technology. This result shows that the nuclear-induced spectral diffusion must be suppressed by another method, in order to implement fault-tolerant quantum computation with isotopically natural silicon.

Chapter 5

Dynamical Decoupling

5.1 Overview

The measured electron spin coherence times for our samples in Chapter 4 are too short to satisfy the error threshold for the fault-tolerant quantum computation. In this chapter, we present an ESR pulse technique, so-called dynamical decoupling, to suppress the spectral diffusion and consequently preserve quantum information in electron spin longer. The performance of dynamical decoupling technique will be evaluated in the prospect of fault-tolerant quantum computation.

5.2 Experimental details

Experimental setup is same to that described in Chap. 4 except that all measurements in this chapter are done for the Si:P sample with the donor

density of $1.1 \times 10^{17}\, cm^{-3}$. Dynamical decoupling (DD) measurements, extended version of the Hahn echo decay measurement in Chapter 4, were performed.

For understanding, equidistant pulse schemes for dynamical decoupling are shown in Fig. 5.1. Carr and Purcell first showed that the compressed exponential factor in the echo decay can be suppressed using multiple spin-flip (refocusing) pulses [47]. This is based on the fact that the exponent of the compressed exponential factor is non-linear. The Hahn echo sequence, which uses one refocusing pulse, renders the echo decay of $E_1(t) = E(0)\exp\{-\frac{t}{T_2} - \left(\frac{t}{T_{SD}}\right)^n\}$ as described above. On the other hand, when using two equidistant spin-flip pulses, the echo decay is given as $E_2(t) = E_1\left(\frac{t}{2}\right)E_1\left(\frac{t}{2}\right) = E(0)\exp\{-\frac{t}{T_2} - 2\left(\frac{t}{2T_{SD}}\right)^n\}$ for the same total free-precession time t. Similarly, the echo decay is $E_N(t) = \{E_1\left(\frac{t}{N}\right)\}^N = E(0)\exp\{-\frac{t}{T_2} - N\left(\frac{t}{NT_{SD}}\right)^n\}$ for N equidistant spin-flip pulses. It is clear that if $n > 1$, the compressed exponential factor due to the spectral diffusion is suppressed more with increasing N. This pulse technique using multiple spin-flip pulses to suppress spin decoherence, is called dynamical decoupling (DD) [48]-[50].

One important issue with dynamical decoupling is to optimize the

sequence of spin-flip pulses so that its decoherence-suppressing performance is enhanced. Each spin-flip pulse used in dynamical decoupling has inevitable errors in length, height, and shape. These result in additional decoherence; thus, the number of spin-flip pulses must be decreased as much as possible while satisfying the required coherence time. Moreover, suppressing the decoherence at short times (high fidelity regime [51]) is specifically important in fault-tolerant quantum computation. Regarding these requirements, the optimal dynamical decoupling sequence was suggested by Uhrig [50] and many researchers have contributed to verifying the sequence in various systems [51] – [53].

Regarding pulse sequences used in dynamical decoupling experiments, UDD has aperiodic pulse timings: $t_k = tsin^2 \frac{k\pi}{2(N+1)}, where\ k = 1,2,\cdots,N$. On the other hand, periodic dynamical decoupling (PDD) has periodic pulse timings based on the conventional Carr-Purcell-Meiboom-Gill sequence [54]: $t_k = t(2k-1)/2N$. In these equations, t represents the total free-precession time taken for the recovered coherence appears in the form of an echo after the initial coherence is created by a $\frac{\pi}{2}$-pulse.

In the same way as performed in the Hahn echo decay measurement, echo amplitude was measured while changing t for different DD sequences. Unfortunately, the instrumental phase noise, mentioned in Chapter 4,

induced unexpected distortion of echo decay. This effect manifests itself as abnormally large noise in decay curve and a rapid decay at the initial part of echo decay. However this does not harm the core of our results because UDD sequence, which utilizes aperiodic pulse sequence, turns out to be strong for this effect. Detailed discussion on this issue will be given in Section 5.4.

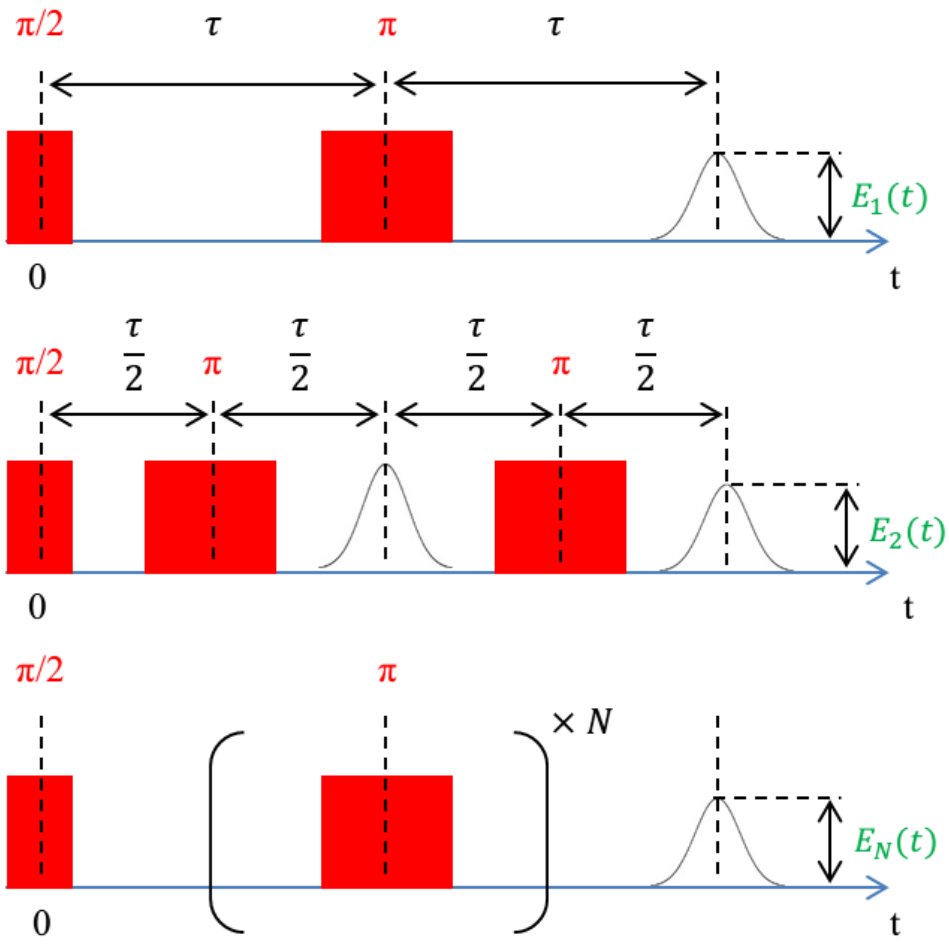

Figure 5.1: Pulse schemes for dynamical decoupling. The uppermost shows the Hahn echo sequence which uses one refocusing pulse (π). The mid shows the dynamical decoupling scheme which uses two equidistant refocusing pulses. The lowest shows the dynamical decoupling scheme with N refocusing pulses.

5.3 Results

Echo decays measured by two different dynamical decoupling schemes, the periodic (equidistant) sequence (PDD) and Uhrig's sequence (UDD), are shown in Fig. 5.2. Note that the sequence with one spin-flip pulse is just the Hahn echo sequence, and that with up to two spin-flip pulses, PDD and UDD use the same sequence. For more than three spin-flip pulses, UDD uses non-equidistant sequences and becomes different from PDD. It is clear that both PDD and UDD do not change the initial exponential factor due to instantaneous diffusion, and do suppress the compressed exponential factor due to the nuclear-induced spectral diffusion described above. To compare the performance of PDD and UDD clearly, T_2 of about $0.9\,\mathrm{ms}$ is obtained by an exponential fit to the initial data for the UDD with seven spin-flip pulses (UDD7). The echo decays are divided by the exponential factor, $\exp(-\frac{t}{0.9\,\mathrm{ms}})$, so that only the compressed exponential factors remain (bottom plots in Fig. 5.2). For the same number of spin-flip pulses, UDD clearly shows better performance than PDD, for suppressing nuclear-induced spectral diffusion. Assuming that the echo decays without the instantaneous diffusion factor can be well expressed by $E_{SD}(t) = \exp\{-\left(\frac{t}{T_{SD}}\right)^n\}$, T_{SD} can be roughly estimated from the time taken

for the decrease of the echo signal to $1/e$ of its initial value. With four spin-flip pulses, for instance, PDD renders about $1.3\,\mathrm{ms}$ for T_{SD} while UDD does about $1.9\,\mathrm{ms}$. These values are longer than T_{SD} ($\sim 0.26\,\mathrm{ms}$) of the Hahn echo sequence by $5-7$ times and thus, if the compression exponent n does not increase, it is still hard to satisfy the requirement for fault-tolerant quantum computation. Many more spin-flip pulses are needed. In Section 5.5, we will show that UDD increases n in our results to satisfy the fault-tolerant error threshold with several spin-flip pulses.

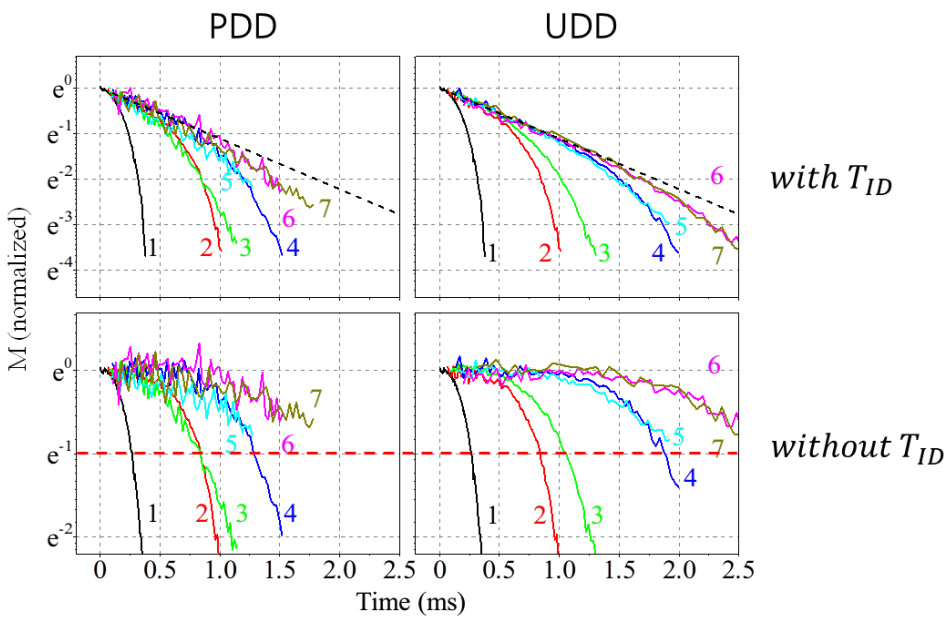

Figure 5.2: Electron spin echo decays measured by two different dynamical decoupling schemes, PDD and UDD. Integer indicates the number of refocusing pulses used for the corresponding echo decay.

5.4 Phase fluctuation and signal mixing

The noise characteristic of the echo decays in Fig. 5.2 has an important implication. In order to learn more about the noise characteristic, the non-normalized echo decays for UDD and PDD with three spin-flip pulses (UDD3, PDD3) were determined, as shown in Fig. 5.3. The noise level of PDD is much greater than that of UDD in spite of the same average value. In addition, the noise level up to the mid-part of the echo decay is much greater than that at the latter part of the decay. Furthermore, the rapid initial decay, ruled out in the normalization process above, is observed for PDD3. All of these characteristics can be understood by considering both the signal mixing of unwanted echoes from a multi-pulse measurement [55] and the instrumental phase noise (Fig. 5.4). For example, the pulse sequences of UDD3 and PDD3 with their relevant echoes are shown in Fig. 5.5, and mechanisms of each echo are summarized in Table 5.1. It is important to note that due to the periodicity of the PDD sequence, one additional echo ($echo_B$) is involved in the signal mixing process for the PDD3 case. This also explains the greater noise level of PDD compared to that of UDD. For the quantum error correction technique required when implementing QIP devices, it is important to know the precise degree of coherence at a certain total precession time. Therefore, we claim that when

adopting a DD sequence, the possibility of additional noise due to the periodicity of the sequence should be considered.

To explain the dependence of the noise level on the total precession time, here we present an analytic model for a simple case of signal mixing concerning two component echoes. Let their amplitudes be A, B and phases θ, φ respectively. Then, the mixed echo amplitude M, measured with the amplitude-average method mentioned above, is given as follows.

$$\frac{\mathrm{M}}{\mathrm{A+B}} = \sqrt{1 + \frac{2a}{(1+a)^2}(f(\theta,\varphi) - 1)}, \tag{2}$$

$$where\ a = \frac{B}{A} < 1\ and\ f(\theta,\varphi) = cos\theta cos\varphi + sin\theta sin\varphi$$

In addition, if the correlation of θ and φ weakens due to instrumental phase noise, the statistical distribution of the signal, M, changes. Therefore, the characteristic of Eq. (2) determines the measured signal strength and noise level. For example, when the intervals between the pulses of DD are much shorter than the correlation time of the instrumental phase noise, which corresponds to several μsec in our equipment, θ and φ are fully correlated; that is, $\theta = \varphi$. In this case, $f(\theta,\varphi) = 1$, and the average of M becomes the maximum value, (A+B). The noise level in this case is also irrelevant with regard to the signal mixing. However, with an increase in the total precession time, the correlation of θ and φ becomes weaker and the

average of M therefore becomes smaller while the dispersion of M increases. These changes in the statistical values of M are responsible for the rapid initial decay and the high noise level in the mid-part observed for PDD3, respectively. In the latter part of the echo decay, the relative magnitudes of the two component echoes, a, play an important role. After one component echo decays more rapidly than the other, that is when $a \ll 1$, the influence of $f(\theta, \varphi)$ is negligible, as is the dispersion of M. As a result, the noise level of the latter part is much smaller than that of other part.

As described above, when the instrumental phase noise and signal mixing occur together during DD measurements, the distortion in the echo amplitude and the amplification of the noise level should be considered. In particular, the fact that this noise amplification manifests more strongly in a periodic DD sequence will be important when adopting a DD sequence to be used in QIP devices. In this regard, it is encouraging that in our results for Si:P, the UDD, which uses a non-periodic sequence, outperforms the PDD in terms of preserving the electron spin coherence.

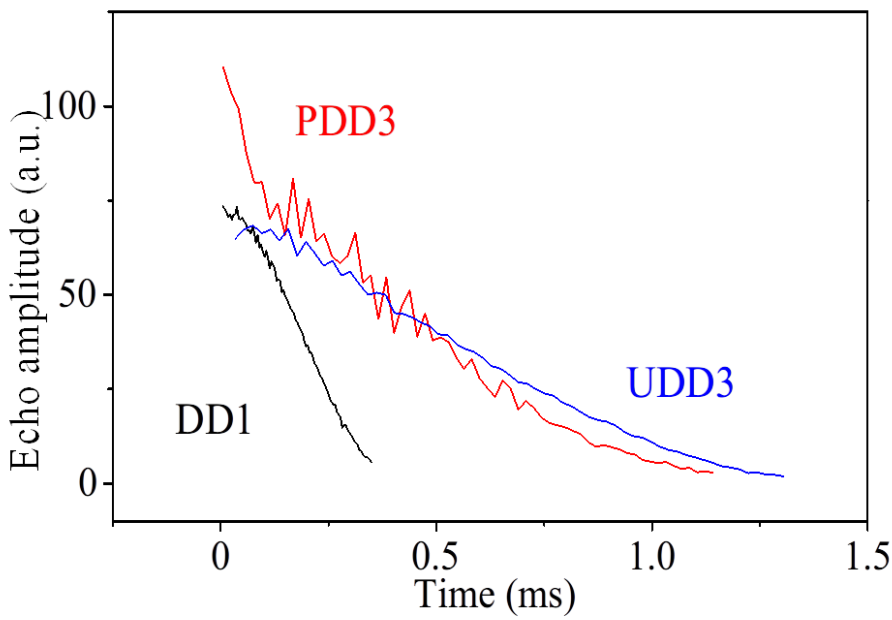

Figure 5.3: Electron spin echo decays obtained by PDD3 and UDD3 schemes. The Hahn echo decay (DD1) is also plotted for comparison. Each data point was obtained by the average of 10 data instances from the magnitude of the echo amplitude.

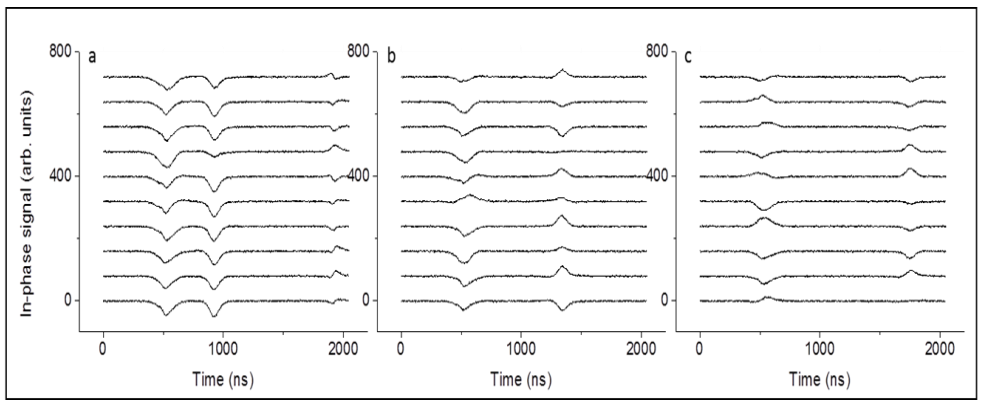

Fig.5.4: Fluctuations of the echo phases due to the instrumental phase noise. Each curve represents the non-averaged echo signals in the time domain after the UDD3 pulse sequence. The total precession times for the first echo (DD main echo) in each graph are (a) 6.8 μs, (b) 13.7 μs, and (c) 20.5 μs, respectively. From the location of the second echo in each graph, the mechanism of its formation can be revealed, as shown in Table 1. When the time intervals of the pulses are greater than several μs, fluctuations of the echo phases occur. In the PDD3 measurements, these two echoes appear at the same position and therefore create the signal mixing effect.

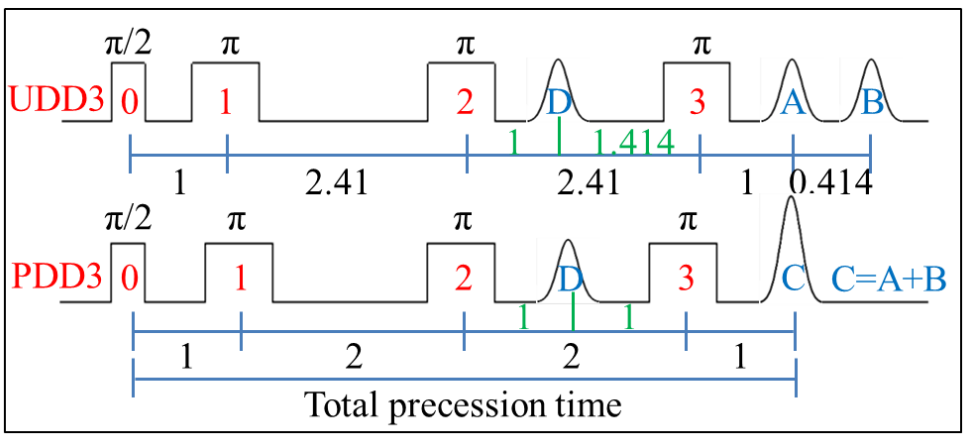

Figure 5.5: Pulse sequences and the related echoes for the PDD3 and UDD3. Note that we assume that the instrumental phase noise is absent here; hence, it appears as if coherent control of the spin-flip pulses (180°) is possible, and all echoes have the same phase. The periodicity of PDD leads to the signal mixing of more echoes. The mechanism of the formation of each echo is summarized in Table 5.1.

5.5 Reliable storage of quantum information

The echo decays divided by the exponential factor for some DD sequences are compared in Fig. 5.6. There, the time scale of each echo decay is normalized to the corresponding T_{SD} value obtained by fitting the data to the equation $E_{SD}(t) = \exp\{-\left(\frac{t}{T_{SD}}\right)^{n}\}$. Compared to the Hahn echo sequence (DD1), UDD with four spin-flip pulses (UDD4) clearly shows better performance in suppressing the decoherence at short times, while PDD3 shows no significant difference. We note that the shape of the echo decay on the normalized time scale can be represented by the fitting parameter n; moreover, the higher n corresponds to less decay, that is, less decoherence, at short times. The values of n for different DD sequences are shown in the inset of Fig. 5.6. Here we exclude PDD data with more than four spin-flip pulses, and UDD7 because the corresponding echo decays do not give reasonable fitting results due to their low signal to noise ratio (SNR). This SNR results from the mixing of the primary echo and the secondary echoes in the presence of the instrumental phase noise (see Supplementary Information). Though the dependence of n on the number of spin-flip pulses is not clear here, we can safely say that UDD renders higher n than do the Hahn echo sequence and PDD. According to the simulation result of

$echo_A$	0-1-(Hahn)-2-(Hahn)-3-(Hahn) (DD main echo)
	0-1-3-(Stimulated)
	0-2-(Hahn)
$echo_B$	0-1-2-(Stimulated, $echo_D$)-3-(Hahn)
$echo_C$	Mixing of ($echo_A$) and ($echo_B$)

Table 5.1: Mechanism of the formation of the echoes shown in Fig. 5.5. The integer indicates the associated pulse in Fig. 3. There are two basic mechanisms here. 1) The two-pulse Hahn echo ($90^\circ - \tau - \theta - \tau$ -echo) and 2) the three-pulse stimulated echo ($90^\circ - \tau - \theta$ -T- $\theta - \tau$ -echo), where τ and T indicate the time delays between the pulses.

Uhrig, n should increase with the number of spin-flip pulses in UDD [50]. The discrepancy between the two results may be due to the imperfection of real pulses, especially errors in the pulse phase of our system, which leads to the degradation of DD sequence increasing with the number of spin-flip pulses.

It is worth checking to see if the suppression of decoherence via the UDD scheme is enough to satisfy the fault-tolerant error threshold. For UDD with four spin-flip pulses (UDD4), the measured values of T_{SD} and n are about 1.9 ms and 5.2, respectively. In the same way as applied to the Hahn echo decay above, the time taken for the increase of the error probability to 10^{-5} is estimated to be about 0.18 ms, which is larger than the 3.7 μs of the

Hahn echo decay by two orders of magnitude. Moreover, even for the error threshold of 10^{-6} required for the fault-tolerant integer factorization [46], the relevant time is estimated to be as long as **0.13 ms**. If we use a **0.1 ms** gating pulse, the required accuracy in pulse length is **0.1 ns**. This level of accuracy is available from commercial GHz pulse generators. This result implies that UDD schemes with a relatively small number of spin-flip pulses, make it possible to satisfy the severe requirement of quantum error-correction by suppressing decoherence due to ^{29}Si impurities in isotopically natural silicon.

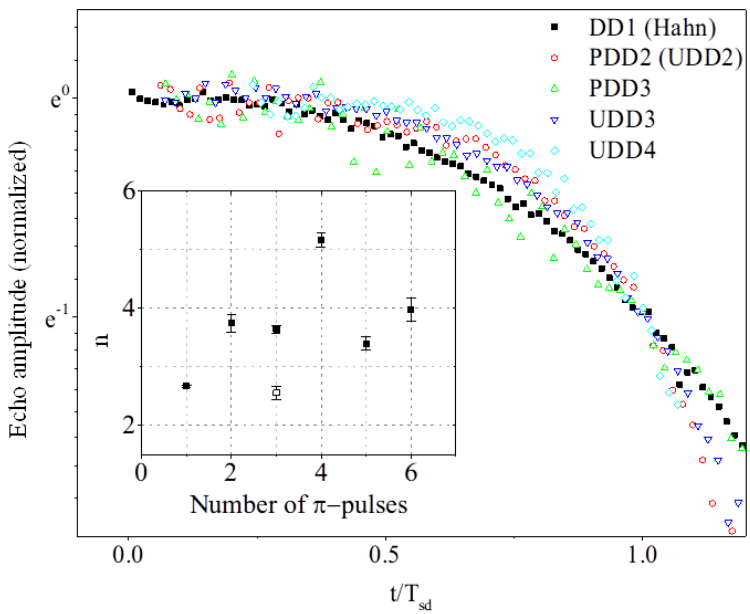

Figure 5.6: Performance of dynamical decoupling at short times. Some of the data of Fig.2(d–e) are plotted on the normalized time scale. The difference in the shape of the echo decay between DD schemes implies that UDD outperforms DD1 (the Hahn echo sequence) and PDD at short times. The shape of the echo decay can be represented by the fitting parameter **n** and the dependence of **n** on the number of spin–flip pulses in UDD (closed square) and PDD (open square) schemes is shown in the inset. Note that, up to two spin–flip pulses, both DD schemes use the same sequence.

Chapter 6

Conclusions

In this study, electron spin resonance experiments were performed for dielectric Si:P with the donor density of $6.52 \times 10^{16}\ /cc$ and 1.1×10^{17} to investigate electron spin dynamics in a bath of donor electrons and ^{29}Si nuclear spins.

A CW-ESR experiment on phosphorus donor electrons of isotopically natural silicon with the donor density of $6.52 \times 10^{16}\ /cc$ was performed at low temperatures from 0.8 K to 4.7 K and high magnetic field of about 4.6 T. We could obtain preliminary data for dynamic nuclear polarization of ^{31}P and ^{29}Si by spectral hole-burning measurements. By measuring hole depth during burning hole at L-line, time dependence of ^{29}Si DNP build-up was found to be biexponential. This biexponential behavior can be explained by a two-step process: DNP build-up in the vicinity of donors and then nuclear spin diffusion into region far from donors. The observed dependence of time constants on excitation power supports this explanation. By

measuring hole depth after burning hole at L-line, time constants of relaxation of ^{29}Si DNP were obtained. The relaxation process showed biexponential time dependence, however time constants could not be extracted reliably, neccesitating further study to clarify relevant relaxation mechanisms.

A pulsed-ESR experiment on phosphorus donor electrons of isotopically natural silicon with the donor density of $6.52 \times 10^{16}\ /cc$ was performed at low temperatures from 4 K to 22 K and high magnetic field of about 3.4 T. The measured temperature dependence of time constants of longitudinal and transverse relaxations agrees with the previous results. In particular, at temperatures lower than about 11 K, longitudinal relaxation was found to be negligible compared to transverse relaxation. To investigate spin decoherence which causes transverse relaxation, a Hahn echo decay of isotopically natural silicon with the phosphorus donor density of $1.1 \times 10^{17}\ /cc$ at 4 K was analyzed. The measured echo decay has a form of the product of single exponential factor and compressed exponential factor as expected. The extracted time constants, T_2 of 0.9 ms and T_{SD} of 0.26 ms, can be explained by instantaneous diffusion and (^{29}Si) nuclear-induced spectral diffusion, respectively. It was also verified that the presence of ^{29}Si nuclei in lattice suppresses flip-flops of electron spins. The measured T_{SD}

(0.26 ms) and n (2.7) cannot satisfy the requirement for fault-tolerant quantum computation.

A dynamical decoupling experiment on the sample with $1.1 \times 10^{17}\ P/cc$ was performed at 4 K. This was to check if dynamical decoupling can suppress spectral diffusion so that preserved spin coherence satisfies the requirement for fault-tolerant quantum computation. The theoretically driven optimal DD sequence, UDD, showed better performance than the equidistant DD sequence, PDD in prolonging coherence time. UDD also showed remarkable performance of suppressing spectral diffusion at short times (high fidelity regime), verified in the change of echo decay shape. UDD with four spin-flip pulses rendered T_{SD} of 1.9 ms and n of 5.2, which corresponds to 0.13 ms for reliable storage of quantum information, satisfying the error threshold of 10^{-6} required for fault-tolerant integer factorization.

It should be noted that the remaining decoherence, instantaneous diffusion arising from ensemble measurement, must be handled using other solutions. Simultaneous manipulation of multiple physical qubits is necessary for quantum error-correction; thus, physical qubits composing a logical qubit should be arranged carefully to avoid instantaneous diffusion. Furthermore, in the silicon electronic devices proposed for implementing quantum

computers, additional decoherence may arise from the surface [56]. Therefore, further study will be required to determine if dynamical decoupling is effective for that kind of decoherence.

References

[1] R. C. Fletcher, W. A. Yager, G. Lo Pearson, A. N. Holden, W. T. Read, and F. R. Merritt, "Spin resonance of donors in silicon," *Phys. Rev.*, vol. 94, no. 5, p. 1392, 1954.

[2] G. Feher and E. A. Gere, "Electron Spin Resonance Experiments on Donors in Silicon. II. Electron Spin Relaxation Effects," *Phys. Rev.*, vol. 114, no. 5, pp. 1245 – 1256, 1959.

[3] G. Feher, "Electron Spin Resonance Experiments on Donors in Silicon. I. Electronic Structure of Donors by the Electron Nuclear Double Resonance Technique," *Phys. Rev.*, vol. 114, no. 5, pp. 1219 – 1244, 1959.

[4] D. Wilson and G. Feher, "Electron Spin Resonance Experiments on Donors in Silicon. III. Investigation of Excited States by the Application of Uniaxial Stress and Their Importance in Relaxation Processes," *Phys. Rev.*, vol. 124, no. 4, pp. 1068 – 1083, 1961.

[5] J. P. Gordon and K. D. Bowers, "Microwave spin echoes from donor electrons in silicon," *Phys. Rev. Lett.*, vol. 1, no. 10, p. 368, 1958.

[6] J. Klauder and P. Anderson, "Spectral Diffusion Decay in Spin Resonance Experiments," *Phys. Rev.*, vol. 125, no. 3, pp. 912 – 932, 1962.

[7] M. Chiba and A. Hirai, "Electron spin echo decay behaviours of phosphorus doped silicon," *J. Phys. Soc. Japan*, 1972.

[8] B. E. Kane, "A silicon-based nuclear spin quantum computer," pp. 133 – 137, 1998.

[9] A. M. Tyryshkin, J. J. L. Morton, S. C. Benjamin, A. Ardavan, G. A. D. Briggs, J. W. Ager, and S. A. Lyon, "Coherence of spin qubits in silicon," *J. Phys. Condens. Matter*, vol. 18, no. 21, p. S783, 2006.

[10] W. M. Witzel, M. S. Carroll, A. Morello, Ł. Cywiński, and S. Das Sarma, "Electron Spin Decoherence in Isotope-Enriched Silicon," *Phys. Rev. Lett.*, vol. 105, no. 18, p. 187602, Oct. 2010.

[11] K. Saeedi, S. Simmons, J. Z. Salvail, P. Dluhy, H. Riemann, N. V Abrosimov, P. Becker, H.-J. Pohl, J. J. L. Morton, and M. L. W. Thewalt, "Room-temperature quantum bit storage exceeding 39 minutes using ionized donors in silicon-28," *Science (80-.).*, vol. 342, no. 6160, pp. 830 – 833, 2013.

[12] J. T. Muhonen, J. P. Dehollain, A. Laucht, F. E. Hudson, R. Kalra, T. Sekiguchi, K. M. Itoh, D. N. Jamieson, J. C. McCallum, and A. S. Dzurak, "Storing quantum information for 30 seconds in a nanoelectronic device," *Nat. Nanotechnol.*, vol. 9, no. 12, pp. 986 – 991, 2014.

[13] H. Tezuka, A. R. Stegner, A. M. Tyryshkin, S. Shankar, M. L. W. Thewalt, S. A. Lyon, K. M. Itoh, and M. S. Brandt, "Electron paramagnetic resonance of boron acceptors in isotopically purified silicon," *Phys. Rev. B*, vol. 81, no. 16, 2010.

[14] D. P. DiVincenzo and others, "The physical implementation of quantum computation," *Fortschritte der Phys.*, vol. 48, pp. 771 – 783, 2000.

[15] D. P. DiVincenzo, D. Bacon, J. Kempe, G. Burkard, and K. B. Whaley, "Universal quantum computation with the exchange interaction," *Nature*, vol. 408, no. 6810, pp. 339 – 342, 2000.

[16] B. Koiller, X. Hu, and S. Das Sarma, "Exchange in silicon-based quantum computer architecture," *Phys. Rev. Lett.*, vol. 88, pp. 279031 – 279034, 2002.

[17] I. Appelbaum, B. Huang, and D. J. Monsma, "Electronic measurement and control of spin transport in silicon," *Nature*, vol. 447, no. 7142, pp. 295 – 298, 2007.

[18] T. D. Ladd, F. Jelezko, R. Laflamme, Y. Nakamura, C. Monroe, and J. L. O'Brien, "Quantum computers," *Nature*, vol. 464, no. 7285, pp. 45 – 53, 2010.

[19] W. O'Mara, R. B. Herring, and L. P. Hunt, *Handbook of semiconductor silicon technology*. Crest Publishing House, 2007.

[20] E. Abe, K. M. Itoh, J. Isoya, and S. Yamasaki, "Electron spin phase relaxation of phosphorus donors in nuclear spin enriched silicon," pp. 1 – 5, 2008.

[21] E. Abe, J. Isoya, and K. M. Itoh, "Pulsed EPR study of spin coherence time of P donors in isotopically controlled Si," *Phys. B Condens. Matter*, vol. 376, pp. 28 – 31, 2006.

[22] J. M. Luttinger and W. Kohn, "Motion of electrons and holes in perturbed periodic fields," *Phys. Rev.*, vol. 97, no. 4, p. 869, 1955.

[23] W. Kohn and J. M. Luttinger, "Theory of donor states in silicon," *Phys. Rev.*, vol. 98, no. 4, p. 915, 1955.

[24] R. L. Aggarwal and A. K. Ramdas, "Optical determination of the symmetry of the ground states of group-V donors in silicon," *Phys. Rev.*, vol. 140, no. 4A, p. A1246, 1965.

[25] C. J. Wellard, L. C. L. Hollenberg, F. Parisoli, L. M. Kettle, H.-S.-S. Goan, J. a. L. McIntosh, and D. N. Jamieson, "Electron Exchange

Coupling for Single Donor Solid-State Qubits," *Phys. Rev. B*, vol. 68, no. 19, p. 10, 2003.

[26] L. M. Kettle, H.-S. Goan, S. C. Smith, L. C. L. Hollenberg, and C. J. Wellard, "The effects of J-gate potential and interfaces on donor exchange coupling in the Kane quantum computer architecture," *J. Phys. Condens. Matter*, vol. 16, no. 7, pp. 1011–1023, Feb. 2004.

[27] D. New and T. G. Castner, "Donor clusters in silicon. Results of ESR measurements," *Phys. Rev. B*, vol. 29, no. 4, pp. 2077–2087, 1984.

[28] R. A. Faulkner, "Higher donor excited states for prolate-spheroid conduction bands: a reevaluation of silicon and germanium," *Phys. Rev.*, vol. 184, no. 3, p. 713, 1969.

[29] F. Bloch and I. I. Rabi, "Atoms in variable magnetic fields," *Rev. Mod. Phys.*, vol. 17, no. 2–3, pp. 237–244, 1945.

[30] A. Honig, "Polarization of arsenic nuclei in a silicon semiconductor," *Phys. Rev.*, vol. 96, no. 1, p. 234, 1954.

[31] D. Pines, J. Bardeen, and C. Slichter, "Nuclear Polarization and Impurity-State Spin Relaxation Processes in Silicon," *Phys. Rev.*, vol. 106, no. 3, pp. 489–498, 1957.

[32] E. Abrahams, "Donor electron spin relaxation in silicon," *Phys. Rev.*, vol. 107, no. 2, p. 491, 1957.

[33] F. Bloch, "Nuclear induction," *Phys. Rev.*, vol. 70, no. 7–8, p. 460, 1946.

[34] M. Song, M. Jeong, T. Ueno, B. Kang, K. Sugiyama, K. Tanaka, A. Matsubara, S. Lee, S. Mitsudo, and T. Mizusaki, "High field ESR of P-doped Si for Quantum Computing Application," in *Journal of Physics: Conference Series*, 2009, vol. 150, no. 2, p. 22078.

[35] T. Maly, G. Debelouchina, and V. Bajaj, "Dynamic nuclear polarization at high magnetic fields," *J. …*, vol. 128, no. 5, pp. 1 – 39, 2008.

[36] A. Tyryshkin, S. S. Lyon, A. Astashkin, and a. A. Raitsimring, "Electron spin relaxation times of phosphorus donors in silicon," *Phys. Rev. B*, vol. 68, no. 19, p. 193207, Nov. 2003.

[37] M. Song, M. Jeong, B. Kang, S. Lee, T. Ueno, A. Matsubara, T. Mizusaki, Y. Fujii, S. Mitsudo, and M. Chiba, "Spin dynamics of isolated donor electrons in phosphorus-doped silicon from high-frequency electron spin resonance.," *J. Phys. Condens. Matter*, vol. 22, no. 20, p. 206001, May 2010.

[38] T. Castner, "Raman Spin-Lattice Relaxation of Shallow Donors in Silicon," *Phys. Rev.*, vol. 130, no. 1, pp. 58 – 75, 1963.

[39] R. Orbach, "Spin-Lattice Relaxation in Rare-Earth Salts," *Proc. R. Soc. A Math. Phys. Eng. Sci.*, vol. 264, no. 1319, pp. 458 – 484, 1961.

[40] A. M. Tyryshkin, S. Tojo, J. J. Morton, H. Riemann, N. V Abrosimov, P. Becker, H. J. Pohl, T. Schenkel, M. L. Thewalt, K. M. Itoh, and S. A. Lyon, "Electron spin coherence exceeding seconds in high-purity silicon," *Nat Mater*, vol. 11, no. 2, pp. 143 – 147, 2012.

[41] G. Zhidomirov and K. Salikhov, "CONTRIBUTION TO THE THEORY OF SPECTRAL DIFFUSION IN MAGNETICALLY DILUTED SOLIDS," *… Exp. Theor. …*, vol. 29, no. 6, pp. 7 – 10, 1969.

[42] R. de Sousa and S. Das Sarma, "Electron spin coherence in semiconductors: Considerations for a spin-based solid state quantum computer architecture," *Phys. Rev. B*, vol. 67, no. 3, p. 33301, Jan. 2003.

[43] E. Abe, A. M. Tyryshkin, S. Tojo, J. J. L. Morton, W. M. Witzel, A. Fujimoto, J. W. Ager, E. E. Haller, J. Isoya, S. a. Lyon, M. L. W. Thewalt, and K. M. Itoh, "Electron spin coherence of phosphorus donors in silicon: Effect of environmental nuclei," *Phys. Rev. B - Condens. Matter Mater. Phys.*, vol. 82, pp. 9 – 12, 2010.

[44] K. Andres, R. N. Bhatt, P. Goalwin, T. M. Rice, and R. E. Walstedt, "Low-temperature magnetic susceptibility of Si: P in the nonmetallic region," *Phys. Rev. B*, vol. 24, no. 1, pp. 244 – 260, 1981.

[45] K. M. Salikhov, S.-A. Dzuba, and A. M. Raitsimring, "The theory of electron spin-echo signal decay resulting from dipole-dipole interactions between paramagnetic centers in solids," *J. Magn. Reson.*, vol. 42, no. 2, pp. 255 – 276, 1981.

[46] J. Preskill, "Reliable quantum computers," *Proc. R. Soc. London. Ser. A Math. Phys. Eng. Sci.*, vol. 454, no. 1969, pp. 385 – 410, 1998.

[47] H. Y. Carr and E. M. Purcell, "Effects of Diffusion on Free Precession in Nuclear Magnetic Resonance Experiments," *Phys. Rev.*, vol. 94, no. 3, pp. 630 – 638, May 1954.

[48] L. Viola, E. Knill, and S. Lloyd, "Dynamical decoupling of open quantum systems," *Phys. Rev. Lett.*, vol. 82, no. 12, p. 2417, 1999.

[49] O. Kern and G. Alber, "Controlling quantum systems by embedded dynamical decoupling schemes," *Phys. Rev. Lett.*, vol. 95, no. 25, p. 250501, 2005.

[50] G. Uhrig, "Keeping a Quantum Bit Alive by Optimized π -Pulse Sequences," *Phys. Rev. Lett.*, vol. 98, no. 10, 2007.

[51] M. J. Biercuk, H. Uys, A. P. VanDevender, N. Shiga, W. M. Itano, and J. J. Bollinger, "Optimized dynamical decoupling in a model quantum memory," *Nature*, vol. 458, no. 7241, pp. 996 – 1000, 2009.

[52] J. Du, X. Rong, N. Zhao, Y. Wang, J. Yang, and R. B. Liu, "Preserving electron spin coherence in solids by optimal dynamical decoupling," *Nature*, vol. 461, no. 7268, pp. 1265–1268, 2009.

[53] Z.-H. Wang, G. De Lange, D. Riste, R. Hanson, and V. V Dobrovitski, "Comparison of dynamical decoupling protocols for a nitrogen-vacancy center in diamond," *Phys. Rev. B*, vol. 85, no. 15, p. 155204, 2012.

[54] S. Meiboom and D. Gill, "Modified Spin-Echo Method for Measuring Nuclear Relaxation Times," *Rev. Sci. Instrum.*, vol. 29, no. 8, p. 688, 1958.

[55] I. Solomon, "Multiple Echoes in Solids," *Phys. Rev.*, vol. 110, no. 1, pp. 61–65, 1958.

[56] T. Schenkel, J. A. Liddle, A. Persaud, A. M. Tyryshkin, S. A. Lyon, R. De Sousa, K. B. Whaley, J. Bokor, J. Shangkuan, and I. Chakarov, "Electrical activation and electron spin coherence of ultralow dose antimony implants in silicon," *Appl. Phys. Lett.*, vol. 88, no. 11, p. 112101, 2006.

요약문

인 도핑된 실리콘에 대한 전자 스핀 동역학 연구

곽 민 찬

물리·천문학부

서울대학교 대학원

양자 전산의 기본 단위인 양자 비트(qubit)에 저장된 양자 정보는 외부와의 상호 작용에 취약하여 시간이 지남에 따라 사라진다. 이러한 단점을 극복하기 위하여 quantum error correction 기법이 연구되었으며, 주어진 조건을 만족시킬 때 이론적으로 임의의 긴 시간 동안 양자 전산을 행할 수 있음이 알려져 있다. 이 때의 조건은 물리적인 qubit의 개수를 임의로 늘릴 수 있어야 하며 (scalability), 한 번의 게이트 연산에 대해 에러가 발생할 확률이 일정 수준 (10^{-4}~10^{-6}) 보다 작아야 한다는 것이다. 이러한 조건들을 만족시킬 수 있는 시스템으로서 Kane에 의해 제안된 실리콘 기반의 핵 스핀 양자 컴퓨터 모델은 실용적인 양자 컴퓨터 구현의 유력한 후보로서 주목 받아왔다. 이에 따라 핵 스핀에 비해 상대적으로

짧은 전자 스핀의 결맞음 시간이 quantum error correction에서 제시하는 조건들을 만족시킬 수 있느냐가 중요한 관건이 되고 있다. 그간의 연구들은 전자 스핀의 결맞음 시간을 늘리기 위하여 도핑 농도와 spin-1/2 ^{29}Si 불순물의 농도를 매우 낮춘 시료들에 대해 주로 이루어졌다. 하지만 두 (전자 스핀) qubit 간의 연산 속도가 exchange constant (J)에 비례한다는 점을 고려하면, 도핑 농도가 높은 시료에 대한 연구가 필요하다.

이 연구에서는 도핑 농도가 각각 $6.52 \times 10^{16}\, cm^{-3}$, $1.1 \times 10^{17}\, cm^{-3}$ 인 isotopically natural Si:P 시료들에 대하여 전자 스핀 공명 (electron spin resonance, ESR) 실험을 통해 전자 스핀의 완화 시간 및 관련 기작들을 규명하고, dynamical decoupling pulse sequence를 사용하여 특정 기작을 억제함으로써 결맞음 시간을 연장하여 quantum error correction 기법에서 요구하는 조건을 만족시킬 수 있는지 여부를 밝힌다. Bulk 시료에 대한 측정 결과로부터 단일 스핀의 동역학에 대한 정보를 얻기 위하여, refocusing (π) pulse를 사용한 스핀 에코 측정을 통해 시료 내에 존재하는 4.7% 가량의 스핀-1/2 ^{29}Si 불순물에 기인한 정적 불균일 효과를 제거하였다.

해당 조건에서 전자 스핀의 결맞음을 깨뜨리는 주요 기작들은 instantaneous diffusion과 spectral diffusion이며, 스핀 에코 신호의 시간에 따른 감쇠 곡선으로부터 각 기작에 해당하는 시간 상수($T_{ID} \sim 0.9\, ms, T_{SD} \sim 0.26\, ms$) 들을 추출하였다. Instantaneous diffusion은 dipolar-coupled 전자 스핀들이 마이크로파 펄스에 의해 동시에 회전할 때

발생하며, 그 시간 상수에 대한 기존의 이론식은 $10^{16}\,cm^{-3}$ 이하의 낮은 도핑 농도 조건에서는 다른 측정 결과들과 잘 맞지만, 우리의 시료 농도에 대해서는 측정값과 크게 다른 값($T_{ID,theory}$~$0.02\,ms$) 을 준다. 이러한 차이점은 도핑 농도가 높아짐에 따라 두 전자 스핀 간의 exchange constant (J)의 크기가 전자 스핀-^{31}P 핵 스핀 간의 초미세 상호작용 (A)의 크기보다 더 커지는 exchange-coupled 스핀 쌍의 개수가 늘어나는 것으로부터 정성적으로 설명될 수 있다. 한편, spectral diffusion은 대상 스핀 주변의 다른 스핀들이 실리콘 격자와의 상호작용을 통해 회전 (flip) 하거나, 스핀들 간의 dipolar interaction을 통해 서로 반대방향으로 회전 (flip-flop) 할 때 대상 스핀에 미치는 자기장이 변화함으로써 발생한다. 기존의 연구 결과들과 우리의 측정값을 비교함으로써, ^{29}Si 불순물의 존재로 인한 불균일 효과가 전자 스핀으로 인한 spectral diffusion을 억제하고, 그 결과 ^{29}Si 핵스핀으로 인한 spectral diffusion이 지배적이 됨을 확인하였다. 다음 단계로, 다수의 refocusing (π) 펄스들을 이용한 dynamical decoupling (DD) 기법을 사용함으로써 spectral diffusion으로 인해 발생하는 결깨짐을 억제하고자 하였다. Uhrig에 의해 이론적으로 유도된 최적의 펄스 시퀀스 (UDD)는 기존의 등간격 펄스 시퀀스 (PDD)에 비해 특히 에코 감쇠 곡선 초반부에서 spectral diffusion을 억제하는데 월등한 성능을 보였다. 에코 감쇠 곡선의 초반부는 quantum error correction에서 중요한 'high-fidelity regime'에 해당하므로, 이러한 결과는 양자 전산에서 dynamical decoupling

기법의 효용성을 높인다. 4개의 refocusing (π) 펄스들을 사용한 UDD에 대한 에코 감쇠 곡선으로부터 에러 발생 확률이 10^{-6} 되는 시간이 약 0.13 ms 임을 추정하였으며, 이는 게이트 연산 시간의 한계로 추정되는 0.1 ms와 비슷한 수준으로서 quantum error correction에서 요구하는 조건을 만족시킨다.

주요어 : 인 도핑 실리콘, 전자스핀공명, 스핀 완화, 스핀 에코, 결깨짐, Dynamical decoupling

학 번 : 2009-20392

Curriculum Vitae

Name : Minchan Gwak

Date of Birth : 1983. 10. 5.

Educations

2009. 3. – 2015. 8. Department of physics and astronomy, Seoul National University (M.S. and Ph.D.)

2002. 3. – 2009. 2. Department of physics and astronomy, Seoul National University (B.S.)

Carrer

2011. 9. – 2015. 6. Training student, KBSI

2009. 3. – 2011. 8. Teaching Assistant of general physic lab., SNU

Publications

1. J. Järvinen, J. Ahokas, S. Sheludyakov, O. Vainio, L. Lehtonen, S. Vasiliev, D. Zvezdov, Y. Fujii, S. Mitsudo, T. Mizusaki, M. Gwak, SangGap Lee, Soonchil Lee, and L. Vlasenko, 'Efficient dynamic nuclear polarization of phosphorus in silicon in strong magnetic fields and at low temperatures', Physical Review B 90, 214401 (2014)
2. J. Järvinen, D. Zvezdov, J. Ahokas, S. Sheludyakov, O. Vainio, L. Lehtonen, S. Vasiliev, Y. Fujii, S. Mitsudo, T. Mizusaki, M. Gwak, SangGap Lee, Soonchil Lee, L. Vlasenko, 'Microscopic control of

^{29}Si nuclear spins near phosphorus donors in silicon', submitted to Physical Review Letters (2015).

3, M. Gwak et al., 'Preservation of electron-spin coherence in isotopically natural silicon with high phosphorus content', submitted to Nature (2015).

Academic activities (Poster)

1. M. Gwak et al., Spring Meeting, Korean Physical Society, Korea (2012).
2. M. Gwak et al., Autumn Meeting, Korean Physical Society, Korea (2012).
3. M. Gwak et al., Autumn Meeting, Korean Physical Society, Korea (2013).
4. M. Gwak et al., Spring Meeting, Korean Physical Society, Korea (2014).
5. M. Gwak et al., The 17th International Symposium on the Physics of Semiconductors and Applications, Korea (2014)
6. M. Gwak et al., Spring Meeting, Korean Physical Society, Korea (2015).